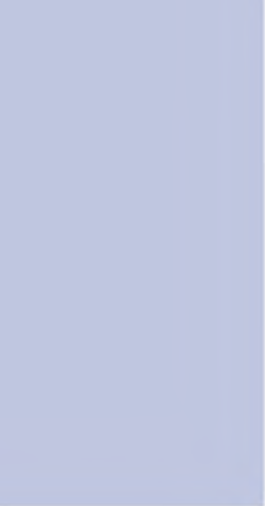


Febex Project Post-mortem Analysis: Corrosion Study



FEBEX Project Post-mortem Analysis: Corrosion Study

V. Madina, I. Azkarate
INASMET

ENRESA
Dirección de Ciencia y Tecnología
Emilio Vargas nº 7
28043 Madrid - España
Tfno.: 915 668 100
Fax: 915 668 169
www.enresa.es

Diseño y producción: TransEdit
Imprime: GRAFISTAFF, S.L.
ISSN: 1134-380X
D.L.: M-53238-2004
Diciembre de 2004

This report has been drawn up within the context of the FEBEX project.
Its contents represents only the opinion of the authors, which do not necessarily coincide
with those of the other participants in the said project.



Table of contents

Table of contents

RESUMEN	1
ABSTRACT	5
1. INTRODUCTION.	9
2. STUDIES CARRIED OUT	13
3. DESCRIPTION OF THE RESULTS	17
3.1 Heater	19
3.1.1 Visual inspection. Extraction of testpieces.	19
3.1.2 Analysis of corrosion products: EDS and XRD	19
3.1.3 Metallographic study performed by optical microscopy.. . . .	19
3.1.4 Evaluation of the hardness of the lid, welded joint and cylinder	19
3.2 Liner	19
3.2.1 Visual inspection	19
3.2.2 Analysis of corrosion products: XRD and EDS	20
3.2.3 Metallographic study performed by Optical Microscopy	20
3.3 Corrosion coupons.	20
3.3.1 Description	20
3.3.2 Visual inspection	20
3.3.3 Rack R1C (M24-01): TStE355 steel	21
3.3.4 Rack R2C (M24-01): AISI 316L steel	21
3.3.5 Rack R3C (M24-02): Titaniums	21
3.3.6 Rack R4C: Coppers.	21
3.3.7 Determining the corrosion rate undergone by the corrosion coupons.	22
3.4 Sensors	22
3.4.1 Extensometer type sensors: SH-SD1-01 and SH-SD1-02	23

3.4.1.1	Visual inspection	23
3.4.1.2	Analysis of corrosion products and/or deposits: EDS and XRD	23
3.4.1.3	Metallographic study performed by optical and scanning electron microscopy	24
3.4.1.4	Chemical analysis of the straight tube and plate	24
3.4.2	Thermocouple type sensors: TSE1-2 and TSD1-11	24
3.4.2.1	Visual inspection	24
3.4.2.2	Analysis of corrosion products and/or deposits: EDS	25
3.4.2.3	Metallographic study performed by optical and scanning electron microscopy	25
3.5	Bentonite.	25
3.5.1	Visual examination	25
3.5.2	Determination of the humidity content	25
3.5.3	Chemical characterisation of bentonites	26
3.5.4	Microbiological characterisation of the bentonite.	26
4.	ANALYSIS OF THE RESULTS	73
	Heater.	75
	Liner	75
	Corrosion coupons	75
	Sensors	75
	Bentonite	76
5.	CONCLUSIONS	79
	Heater.	81
	Liner	81
	Corrosion Coupons	81
	Sensors	81
6.	ANNEX	83



Resumen



Resumen

El desmantelamiento parcial del experimento "in situ" FEBEX fue llevado a cabo durante el verano de 2002, tras 5 años de calentamiento continuo. La operación incluyó la demolición del tapón de hormigón y la retirada de la sección del experimento correspondiente al primer calentador. Durante el desmantelamiento se tomaron un gran número de muestras de todo tipo de materiales para su posterior análisis.

Parte de las muestras recogidas estaban destinadas al análisis de los procesos de corrosión sufridos durante la primera fase operacional del experimento.

Estas muestras comprendían probetas de corrosión de distintos metales instaladas ex profeso, sensores recuperados durante el desmantelamiento que se encontraban seriamente corroídos y bentonita en contacto con dichos sensores. Además se llevó a cabo el estudio de corrosión del calentador extraído y de una sección del tubo guía que lo rodeaba. Todos los análisis fueron llevados a cabo por la Fundación INASMET (España).

Este informe describe en detalle los estudios realizados en los distintos materiales y los resultados obtenidos, así como las conclusiones extraídas.



Abstract



Abstract

The partial dismantling of the FEBEX “in situ” test was carried out during the summer of 2002, following 5 years of continuous heating. The operation included the demolition of the concrete plug and the removal of the section of the test corresponding to the first heater. A large number of samples from all types of materials have been taken during the dismantling for subsequent analysis.

Part of the samples collected were devoted to the analysis of the corrosion processes occurred during the first operational phase of the test. These samples

comprised corrosion coupons from different metals installed for that purpose, sensors retrieved during the dismantling that were found severely corroded and bentonite in contact with those sensors. In addition, a corrosion study was performed on the heater extracted and on one section of liner surrounding it. All the analyses were carried out by the Fundación INASMET (Spain).

This report describes, in detail the studies carried out on the different materials and the obtained results, as well as the drawn conclusions.



1. Introduction



1. Introduction

AITEMIN requested the INASMET Foundation to carry out the tasks laid down in quotation Ref. 73.1707.2, consisting of a study of the corrosion suffered by different components of the “in situ” test of the FEBEX Project being carried out by AITEMIN in Grimsel (Switzerland).

This task was approached in the context of the FEBEX Project, whose aim is to show the feasibility of manufacturing, handling and assembling engineering barriers and developing codes to evaluate the thermo-hydro-mechanical behaviour of the near field of a deep geological repository for high activity radioactive waste. The heaters (two) were installed horizontally using guide tubes (liners), surrounded by bentonite blocks in which test samples were arranged, as well as a series of sensors to monitor different physiochemical parameters.

The test began in July 1996 and, after approximately six years, one of the heaters, a section of guide tube (liner), samples and four sensors were extracted in June 2002. These elements were the object of the study, the aim of which was to evaluate the behaviour of the above-mentioned elements in relation to the corrosion phenomena suffered in the same conditions as those predicted for deep geological disposal in a granitic formation.

Below we give a brief description of the characteristics of the elements studied:

1. Heater

A carbon steel cylinder with welded lids, approximately 4.54 metres long, 0.9 metres in diameter and with a wall thickness of 100 mm, with a total weight of approximately 11 t. The heater sample studied was a section taken from one of its ends, consisting of the lid with its welded joints and a 300 mm section of the body or cylinder.

2. Liner

The guide tube or “liner” consists of a perforated steel tube 970 mm in diameter and 15 mm thick used to make construction of the storage receptacle easier and facilitate insertion of the container in its storage position. The guide tube used in the test consists of 11 segments each 1 metre long, joined to

each other by a machined joint on the edge of each segment that allows them to be fitted 100 mm into each other. The sample sent to INASMET consists of one of these guide tube sections.

3. Corrosion coupons

Coupons of different candidate metals for manufacturing the high activity containers were placed in the clay barrier in order to evaluate their behaviour when faced with corrosion phenomena. The test samples consisted of different-sized parallelepipeds made of the following materials: type TStE355 carbon steel, AISI 316L quality austenitic stainless steel, grade 2, 7 and 12 titanium alloys, pure Cu-ETP copper and the 70/30 and 90/10 cupro-nickel alloys. With the steels and titanium alloys, some of the samples contained welded joints formed using the following techniques: EBW, FCAW and MAGW for the carbon steel, EBW and GTAW for the stainless steel and EBW and PAW for the titaniums. The welded joints and machining of the samples were carried out at INASMET in April 1996. Three complete sets were sent to ENRESA for the FEBEX Project, two for the “in situ” test and a third for that of the model.

4. Sensors

These were part of the instrumentation used to monitor signals for different parameters in the “in situ” test. The samples studied consisted of two extensometer type sensors, used to measure displacement of the heaters (code SH) and two thermocouple type sensors for measuring temperature (code T). With all four sensors, the active element was protected by an austenitic alloy tube or sheath.

5. Bentonite

As the sealing and packing component of the medium in the Engineered Barrier System (EBS), it plays an important role in the corrosion resistance of the materials that it envelops or covers. A chemical and microbiological analysis of the bentonite has been included in the present study. The bentonite used in the FEBEX experiment consisted of 88-96% Ca-Mg-montmorillonite. It showed an initial humidity of $13.7\% \pm 1.3\%$.



2. Studies carried out

2. Studies carried out

The above-mentioned samples were received on the premises of Thyssen Ibérica, Andoain (Guipúzcoa), where the container was sectioned, with a 300 mm piece being cut from one of its ends; this piece and the rest of the components were sent to INASMET to be cut into smaller pieces and studied. The surplus from the heater was sent to AITEMIN.

The following studies were carried out:

1. Visual inspection of the components to be studied. Extraction of test pieces.
The components were examined on receipt. The extent and morphology of the corrosion suffered by the component was evaluated. The cuts to be made were decided on, for later study of the cross-sections obtained.
2. Optical and scanning electron microscope study.
Optical and scanning electron microscope techniques were used to study the metallographic test pieces extracted from the different components and to evaluate the microstructure of the

component and the type and extent of corrosion.

3. Chemical characterisation of corrosion products.
In order to characterise the corrosion products and/or deposits chemically, energy dispersive spectrometry (EDS) analyses were carried out, using a microanalyser coupled to the scanning electron microscope (SEM). The molecular formula of said products was determined by means of X-ray diffraction spectroscopy (XRD).
4. Chemical characterisation of the components.
Chemical analyses of certain of the metallic components sent, were carried out in order to determine the type and quality of the alloy being studied.

With the bentonite, EDS chemical characterisation was carried out, as well as chemical analysis of the leachate obtained. The analysis was completed with microbiological characterisation of the bentonite samples.



3. Description of the results



3. Description of the results

The results obtained from the studies carried out on each of the components are described below:

3.1 Heater

3.1.1 Visual inspection. Extraction of test pieces

The heater studied, Ref. MH-01, was received on the Thyssen Ibérica premises in Andoain (Guipúzcoa), where INASMET technical staff supervised a cut that included the heater lid, its welded joints and a section of the body some 300 mm. long.

Figures 1 to 6 show different views of the heater on the Thyssen premises. The lid area was protected during transport from Grimsel by a plastic wrapping with silica gel as the drying agent, meaning that corrosion in this area is less than that seen on the surface freely exposed to the external environment during storage after extraction and transport to the Thyssen Ibérica premises. Examination of the heater showed very slight and apparently uniform overall corrosion of the surface of the container. No pitting or any other signs of localised corrosion were detected.

Figures 5 and 6 show the cuts made in the heater, including the lid, welded joint and body. The different parts obtained, on which the location of the welded joint was marked, can be seen in Figures 7 and 8, now on the INASMET premises. The test pieces used to carry out the study were extracted from these parts.

3.1.2 Analysis of corrosion products: EDS and XRD

The test pieces extracted from the lid and body underwent energy dispersive spectrometry (EDS) microanalysis of the corrosion products generated on the corroded surface. The EDS spectra in Figure 9 show, for both samples, a majority presence of iron, together with those elements typical of bentonite, such as silicon, calcium and aluminium. Chlorine and sulphur were detected in lesser quantities. The corroded surface was analysed using X-Ray Diffraction (XRD) in order to identify the corrosion products generated. The spectrum, shown in Figure 10, detects iron hydroxide with a molecular formula of $\text{Fe}(\text{OH})_3$, as well as some SiO_2 , possibly as a mineral proceeding from the bentonite. It is important to point out, that it is difficult to obtain data using XRD, with

oxide layers as thin as those generated on the surface of the heater.

3.1.3 Metallographic study performed by optical microscopy

The sections extracted from the lid, welded joint and cylinder were prepared metallographically and studied using an optical microscope, after polishing and metallographic etching.

The optical micrograph in Figure 11 shows the outer surface of the heater in a welded area. A thin layer of oxide, with a thickness less than $15\text{ }\mu\text{m}$, can be seen.

The macrograph in Figure 12 shows one of the cross-sections including a welded joint. Study of the base material making up the lid shows, Figure 13, a ferritic microstructure with areas of pearlite-bainite. The cylinder, in Figure 14, also shows a ferrite-pearlite structure with a smaller ferritic grain size. The microstructure of the heat affected zone (HAZ) of the welded joint, basically bainitic, is shown in Figures 15 and 16.

3.1.4 Evaluation of the hardness of the lid, welded joint and cylinder

A Vickers 10 (HV 10) microhardnesses test was carried out, as per ISO 6507.1, on the metallographic preparation shown in macrograph 1.12, including the lid, weld and cylinder. The results obtained are listed on the results sheet table included in the *Anexo*. A coherent increase in the hardness value measured in the heat affected zone (ZAC) and the weld bead was observed, in comparison with the base material making up the lid and cylinder.

3.2 Liner

The sample of liner or perforated guide tube studied consisted of one of the 11 segments that make up the guide tube, identified as ML-02. It was a section of steel 1 metre long, 970 mm in diameter, with a wall thickness of 15 mm.

3.2.1 Visual inspection

The photographs in Figures 17 to 20 show different views of the liner segment studied. There is observed generalised corrosion of the whole external surface of

the component, with the formation of brownish-red corrosion products and remains of the bentonite that surrounded it, [Figure 20](#), and which still remained lodged inside some of the perforations of the component, [Figure 18](#). The technical staff at INASMET marked the lower (GI) and upper (GS) generatrix.

3.2.2 Analysis of corrosion products: XRD and EDS

Energy dispersive spectroscopy (EDS) was used to analyse the corrosion products generated on the external surface of the liner. The EDS spectrum in [Figure 21](#) shows a majority presence of iron, together with elements associated with the bentonite such as silicon, calcium and aluminium.

In order to determine the stoichiometric combination of the corrosion products generated, XRD analysis of the corrosion products generated on the external surface was carried out. The spectrum shown in [Figure 22](#), identifies iron oxide with a formula of FeOOH , as well as mineral species typical of bentonite.

3.2.3 Metallographic study performed by Optical Microscopy

Different sections extracted from the liner were prepared for metallographic study, by embedding them in resin and polishing, to be studied using an optical microscope. The optical micrographs in [Figures 23](#) to [26](#) show the external and internal surfaces of the liner in sections taken from the upper and lower generatrix. The morphology of the corrosion seen is of the type generalised non-uniform, with maximum values of corrosion penetration of approximately 130 microns on the external surface of the two generatrix. The internal surface of the lower generatrix showed a maximum penetration of up to 200 microns. With the lower generatrix, corrosion penetration was less, with values not exceeding 100 microns. Metallographic development of the material making up the liner shows a ferrite-pearlite microstructure typical of carbon steels.

3.3 Corrosion coupons

3.3.1 Description

The corrosion coupons studied consisted of different sized parallelepipeds manufactured from the follow-

ing materials: TStE355 type carbon steel (UNE F 6215), AISI 316L (UNS S31603) austenitic stainless steel, titanium alloys Grade 2 (UNS R50400), 7 (UNS R52400) and 12 (UNS R53400), pure copper Cu-ETP (UNS C11000) and cupronickel alloys 70/30 (UNS C71500) and 90/10 (UNS C70600). In the case of the steels and the titanium alloys, some of the coupons contained joints welded by EBW (Electron Beam Welding), FCAW (Flux Cored Arc Welding) and MAGW (Metal Active Gas Welding) for the TStE355 steel, EBW and GTAW (Gas Tungsten Arc Welding) for the 316L steel, and EBW and PAW (Plasma Arc Welding) for the titaniums. The welding and machining of the corrosion coupons was carried out by INASMET. [Table 1](#) lists the chemical composition of the above-mentioned materials.

Once weighed and measured, the coupons of the same material were placed on Teflon supports separated by Teflon spacers. Each material was assigned a number: 1 for the TStE355 steel, 2 for the 316L steel, 3 for the titanium alloys and 4 for the coppers. For each type of material, 3 units or racks were assembled, differentiated by the letters A, B, and C. Therefore the 3 racks with carbon steel test coupons were identified as 1A, 1B and 1C, reference that was marked on one of the Teflon supports of each rack. This marked support allowed perfect identification of each corrosion coupon, 1A1, 1A2, 1A3, 1A4 and 1A5, for the racks carrying TStE355 steel. The 12 racks were sent to ENRESA in April 1994.

For the “in situ” experiment of the FEBEX Project, the coupons were inserted into the bentonite blocks closest to the heater and at the bottom, [Figures 27](#) and [28](#).

The test pieces remained buried from July 1996 to June 2002, a period of approximately 6 years.

3.3.2 Visual inspection

[Figures 29](#) and [30](#) show the bentonite blocks as received, protected in vacuum packs. The photograph in [Figure 27](#) shows the block of bentonite identified as BS-24-02 after being unpacked, and a diagram showing the location of this block in the FEBEX “in situ” experiment. Two sets of test coupons were housed inside the block, identified as M24-01 by FEBEX, and which correspond to racks R1C (TStE355 steel) and R2C (316L steel). Only rack R4C (copper), identified as M24-01 by FEBEX is housed in the block of bentonite identified as BS-24-3, [Figure 28](#) Rack R3C (titanium), also identified as M24-01 and tested in block BS-24-3, was sent separately.

Table 1
Chemical composition of the materials studied.

Alloy	Element (%)												
	C	Si	Mn	P	S	Mo	Al	Pd	Cr	Ni	Fe	Cu	Ti
TStE355	0.16	0.41	1.5	0.017	0.002		0.004				Rem		
AISI 316L	0.021	0.31	1.3	0.029	0.002	2.2			17.4	11.5	Rem		
TiGr-2	0.005							0,15			0,04		Rem
TiGr-7	0.040												Rem
Ti-Gr12	0.006					0.28				0.79	0,10		Rem
Cu-ETP				<0.01							<0.005	Rem	
Cu30Ni	0.005		0.69	<0.01			<0.01			30.2	0.65	Rem	
Cu10Ni										10		Rem	

* Rem: reminder.

3.3.3 Rack R1C (M24-01): TStE355 steel

This rack consisted of 5 carbon steel coupons: 2 base material coupons, identified as 1C1 and 1C2, and 3 test coupons with welded joints, 1C3 (EBW), 1C4 (FCAW) and 1C5 (MAG). Visual analysis revealed very superficial corrosion of the carbon steel coupons, even with shiny uncorroded zones being observed, [Figures 31 and 32](#).

Metallographic study of tested coupons shows little penetration of the corrosion, with no differences in the extent of the corrosion being noted between the base and welded materials, [Figures 33 and 34](#). Scanning electron microscope (SEM) analysis of the surface of these coupons reveals a poorly adherent and discontinuous layer of oxide, [Figure 35](#). EDS analysis of this oxide, [Figure 36](#), reveals the majority presence of iron and oxygen, with a small amount of chlorine. The XRD spectrum of the sample only detects the substrate (Fe), given the lack of thickness of the oxide layer generated on the surface of the test sample.

3.3.4 Rack R2C (M24-01): AISI 316L steel

This rack consisted of 4 stainless steel coupons: 2 base material coupons identified as 2C1 and 2C2, and 2 welded coupons, 2C3 (EBW) and 2C4 (GTAW). No indications of corrosion were observed in the four

test pieces tested, which presented the same appearance as they did before beginning the “in situ” test, [Figures 37 and 38](#). Only one of the coupons, identified as R2C3, showed some small marks, [Figure 39](#). Scanning electron microscopy examination revealed that said zones were characterised by stains or colour changes on the surface of the metal, with no corrosion penetration of the material being observed, [Figure 40](#).

3.3.5 Rack R3C (M24-02): Titaniums

This rack consisted of 8 coupons: Ti Gr 2 base (3C1), Ti Gr 2 EBW (3C2), Ti Gr 7 base (3C3 and 3C4), Ti Gr 7 EBW (3C5), Ti Gr 7 PAW (3C6), Ti Gr 12 base (3C7) and Ti Gr 12 EBW (3C8). No corrosion at all was observed of the titanium coupons examined, neither generalised nor localised, [Figures 41 to 44](#). However, on all test pieces there were observed the traces left by the Teflon crevice device used with the titanium test pieces. SEM analysis of these zones revealed that, in all cases analysed, they were strips slightly darker than the rest of the metal, with no beginnings of corrosion due to overlapping or crevice being observed, [Figure 44](#).

3.3.6. Rack R4C: Coppers

This rack consisted of 5 coupons: 2 of Cu-ETP copper (4C1 and 4C2), 2 of Cu10Ni cupronickel (4C3

and 4C4) and 1 of Cu30Ni cupronickel (4C5). This rack showed the greatest amount of corrosion of the test pieces making it up, Figure 45. The Cu-ETP coupons showed a dense and not very adherent oxide layer, Figure 46. The EDS and XRD analyses, shown in Figures 50 and 51, respectively, reveal that this oxide corresponds to the molecular cuprite Cu_2O , with other minerals proceeding from the bentonite being detected. A small chlorine peak was also observed.

The Cu10Ni coupons offered a slightly more adherent layer, Figure 47, whose molecular formula also corresponds to cuprite, Figure 55. With respect to the Cu30Ni cupronickel, the test piece examined showed very slight surface oxidation, Figure 48. The micrographs obtained from SEM analysis, in Figures 57 and 58, show the formation of small crystals on the surface of the coupon, principally consisting of chlorine, nickel and copper, EDS spectra in Figures 59 and 60.

3.3.7 Determining the corrosion rate undergone by the corrosion coupons

The corrosion rate was calculated according to the ASTM G31 standard "Standard Practice for Laboratory Immersion Corrosion Testing of Metals", Section 11. It was assumed that the loss of total weight undergone by the test piece was solely due to generalised corrosion and not to local corrosion phenomena. The "average" corrosion rate was calculated using the formula:

$$v.c = (K \times \Delta p) / A \times t \times D \quad \text{ec. 3.1}$$

Where:

K = cte, the value of K is 8.76×10^7 , if the corrosion rate units are expressed in $\mu\text{m}/\text{year}$

Δp = initial weight – weight of descaled test specimen (g)

t = Test duration (hours)

A = Test specimen area (cm^2)

D = Density of metal specimen in g/cm^3

The weight of the coupons tested was determined by descaling, with 5% citric acid for the steels and with 10% sulphuric acid for the coppers and cupronickels. After descaling, coupons were dried and weighed. The data relating to weight difference, test duration, density and the exposed area of the metal were used to calculate the corrosion rate. The values obtained are shown on the attached table. The corrosion rate was only determined for the carbon steel and copper specimens. With the 316L and titanium coupons, the weight of tested specimens (not descaled) was the same as it was before being tested.

The corrosion rate value obtained for the TStE355 steel is the average of 3 descaled test pieces. With the Cu-ETP and Cu10Ni coppers, the corrosion rate value was obtained from a single test piece.

3.4 Sensors

The sensors were part of the instrumentation used to monitor different parameters during the test. The samples studied were two extensometer type sensors, identified as SH-SD1-01 and SH-SD1-02 in the FEBEX experiment, used to measure displacement of the heaters, and two thermocouples type sensors, identified as TSE1-2 and TSD1-11. According to the technical data supplied by FEBEX, the extensometers were protected by an external tube manufactured from AISI 316L stainless steel. With the temperature sensors, the thermocouple wires were kept apart by using a magnesia insulating filling and an outer

Table 2
Generalised corrosion rate values obtained for the corrosion coupons in the FEBEX "in situ" test.

Material	Corrosion rate $\mu\text{m}/\text{year}$
TStE355	0.10
Cu ETP	0.71
Cu10Ni	0.74

sleeve that, according to data supplied by FEBEX, could be either made from 304 or 316L steel. The photograph in [Figure 61](#) shows the initial location of the extensometers in the FEBEX experiment.

3.4.1 Extensometer type sensors: SH-SD1-01 and SH-SD1-02

3.4.1.1 Visual inspection

SH-SD1-01

The macrograph in [Figure 62](#) shows the bentonite block containing the SH-SD1-01 sensor split into two during operations to extract the components. Diffusion of corrosion products proceeding from the sensor can be seen in the bentonite surrounding it. The overall appearance of the sensor studied is shown in the macrograph in [Figure 63.b](#). Two areas of damage were identified and given the references of 1 (close to the rock) and 2 (close to the liner). These zones coincide with the zones of greatest diffusion of corrosion products, as can be seen in the photograph showing the on-site test of the sensor, [Figure 63.a](#).

Macrographs 64 and 65 correspond to zone 1 close to the rock. The corrosion damage is manifested as pitting, sometimes large, on the surface, advancing from the outer to the inner periphery, occasionally perforating the tube wall. The corrosion products generated in this zone are deep green. The morphology of the corrosion observed in zone 2 close to the liner, [Figures 66 to 68](#), is characterised by pitting, also extensive on the surface, sometimes developing beneath pustules or deposits mainly made up of remains of bentonite and corrosion products. The corrosion products generated in this zone are mainly brown-black.

The macrographs in [Figures 69 to 72](#) show details of the device for attaching the sensor to the rock. Significant corrosion damage can be seen on the plates, bolts, screws and other items making up this anchoring device. The corrosion products generated in this area are mostly greenish, except for those components made from carbon steel, which are brown-red. [Figures 70 and 71](#) show the composition of some of the component parts of the anchoring device, determined by the semi-quantitative EDS analysis shown in [Figure 95](#). Analysis of the screws fixing the sensor to the plate ([Figure 64](#)) showed that they were made from carbon steel.

SH-SD1-02

The corrosion damage observed on sensor Ref. SH-SD1-02, a view of which can be seen in macrograph 4.13, coincides in many ways with that on sensor Ref. SH-SD1-02. The corrosion damage was defined in three zones. Zone 1 close to the rock shows extensive surface pitting that perforates the tube. Bright green corrosion products predominate in this zone, [Figure 74](#). In zone 2, [Figures 75 and 76](#), there is observed pitting development beneath the pustules and/or deposits. The corrosion products in this area are dark brown. In zone 3, close to the liner, [Figures 77 and 78](#), there is detected cracking and pitting of the tube.

The corrosion damage observed on the devices for anchoring the sensor to the rock and the liner, is shown in [Figures 79 to 84](#). The plates where it is joined to the rock show significant cracking, and significant generation of reddish corrosion products. The corrosion products generated on the fixing devices are green (when the substrate is stainless steel) and red, when the component is made from carbon steel.

3.4.1.2 Analysis of corrosion products and/or deposits: EDS and XRD

EDS

In order to characterise the corrosion products and/or deposits generated on the two sensors chemically, energy dispersive spectrometry (EDS) analysis was carried out, using a microanalyser coupled to the scanning electron microscope (SEM). The spectra obtained are shown in [Figures 85 to 94](#).

The most significant data of the study carried out is the presence of sulphur in almost all the corrosion products analysed. As well as sulphur, the analyses identify chrome, iron and occasionally nickel, as elements making up the steel, as well as silicon, calcium, magnesium and aluminium, as elements making up the bentonite surrounding the samples.

The EDS analyses carried out on the green corrosion products show the presence of sulphur, sometimes predominant, [Figures 85, 89 and 92](#). Analysis of the reddish corrosion products shows them to be enriched with the element iron, [Figures 88 and 93](#). A significant fact is that analysis of the corrosion products beneath pustules shows calcium enrichment as well as sulphur, [Figure 90](#).

XRD

In order to characterise the nature of the corrosion products generated, X-ray diffraction analysis (XRD) was carried out.

Figure 96 shows the spectrum obtained from analysis of the green corrosion products observed on the surface of the sensor SH-SD1-01. As well as calcite, CaCO_3 , analysis also detected iron sulphide Pyrrhotite, Fe_{1-x}S . XRD analysis carried out on one of the pustules, Figure 97, associates the peaks with calcite.

It must be pointed out that XRD analysis gives us information about crystalline species, these being the ones that refract. Therefore, amorphous compounds, such as most iron sulphates, that not refract, do not therefore appear in the spectrum. In the same way, the height of the peak in an XRD diffractogram indicates the degree of crystallinity of a compound and not of its concentration.

3.4.1.3 Metallographic study performed by optical and scanning electron microscopy

Metallographic probes were prepared from the sections extracted from the corrosion-damaged areas described in the visual inspection section. The metallographic probes thus prepared were examined using optical and scanning electron microscopes, in order to study the morphology and progression of the corrosion, as well as the microstructure of the component materials of the sensors being studied.

The optical micrographs in Figures 98 to 108 show different sections extracted from the two sensors being studied. The samples show significant corrosion penetration of the material, with a clear advance from the outer to the internal periphery. The steel making up the external tube of both sensors shows a non-sensitised austenitic microstructure, with a certain degree of intergranular advance of the corrosion, especially in zones of the tube close to the liner, Figures 100 and 101.

The optical micrograph in Figure 104 shows a cross section of a pustule in zone 2 of the sensor SH-SD1-02. Treatment of said cross section with polarised light, Figure 105, shows a whitish, crystalline precipitate inside that corresponds to the calcite, CaCO_3 , analysed by XRD.

The optical micrographs in Figures 106 to 112 show details of the cracking detected in zone 3 of the sensor SH-SD1-02. The cracks clearly initiate at the outer periphery and have a ramified morphology with transgranular progression. These cracks, typical of stress corrosion cracking of stainless steels, sometimes initiate from pitting on the external surface of the tube.

The optical micrographs in Figures 109 to 113 show different aspects of the morphology of the damage observed in the anchor points of the two sensors to the liner and the rock. Figures 100 and 111 show the cracking detected in fitting securing sensor SH-SD1-02 to the rock. The optical micrograph in Figure 112 shows the corrosion damage produced in one of the carbon steel parts.

Finally the electron micrograph in Figure 113 shows the surface morphology of one of the pits on the sensors being studied. This pit has a shiny (or active) surface and shows a certain intergranular progression of the corrosion.

3.4.1.4 Chemical analysis of the straight tube and plate

Chemical analysis of the outer tube making up the extensometer identified as SH-SD1-01 was carried out, so as to verify that it corresponded to AISI 316 quality steel. Chemical analysis of one of the plates used to secure the sensor SH-SD1-01 to the rock was also carried out. The analysis certificates can be found in the annexe. Based on the results obtained, it should be pointed out that the composition of the tube would correspond to that of an AISI 316L steel. With respect to the plate analysed, the composition obtained would be that of a type 304 and/or 302 stainless steel.

3.4.2 Thermocouple type sensors: TSE1-2 and TSD1-11

3.4.2.1 Visual inspection

Figures 114 and 115 show the general appearance of the two thermocouples studied, as well as a diagram of their location in the "in situ" experiment.

Both thermocouples showed zones of damage characterised by generalised corrosion of their surface, Figures 116 and 117, with the formation of a layer or "film" of green corrosion products. In other zones,

the corrosion damage was characterised by a more localised corrosion morphology, in the form of more or less extensive superficial pitting, with generation of green, yellow and black corrosion products, [Figures 118 and 119](#). Shiny or active areas of corrosion were also observed. The corrosion has advanced from the outer to the internal periphery, to perforate the wall of the tube or sheath covering the sensors, leaving the insulation or magnesia open to view, together with the two wires making up the thermocouple.

3.4.2.2 Analysis of corrosion products and/or deposits: EDS

In order to characterise the corrosion products and/or deposits in the damaged zones of the two thermocouples chemically, semi-quantitative analyses were carried out by means of energy dispersive spectroscopy (EDS), using a microanalyser coupled to the scanning electron microscope (SEM). [Figures 117 and 119](#) show the zones analysed by EDS.

[Figures 120 to 124](#) show the EDS spectra obtained. Sulphur was detected in the green and black corrosion products analysed, [Figures 120 to 122](#). The analyses of the yellow corrosion products showed a significant presence of chlorine and nickel, [Figure 123](#).

Semi-quantitative analysis by means of EDS was carried out on the external tube or sheath of the thermocouples, [Figure 124](#). The spectrum obtained shows that it was a nickel-based alloy.

It was not possible to determine the origin of the titanium detected in certain corrosion products analysed.

3.4.2.3 Metallographic study performed by optical and scanning electron microscopy

Metallographic probes were prepared from sections extracted from the corrosion damaged zones described in the visual inspection section. The metallographic preparations were examined by optical microscopy in order to study the morphology and progression of the corrosion.

The optical micrographs in [Figures 125 to 127](#) show different sections extracted from the thermocouples being studied. The samples show significant corrosion penetration of the material, which has perforated and practically dissolved the outer tube in some sections. The alloy making up the tube or

outer sheath has a somewhat sensitised austenitic structure, however, no intergranular progression of the corrosion was detected.

The SEM micrograph in [Figure 128](#) shows an “active” or shiny surface on one of the thermocouples. A certain degree of intergranular progression of the corrosion can be appreciated.

3.5 Bentonite

As a non-metallic component of the FEBEX experiment, the bentonite plays a decisive role in the corrosion resistance of the materials it surrounds or envelops. Therefore, its chemical and microbiological analysis has been included in the study carried out.

The bentonite used in the FEBEX experiment showed an initial humidity of $13.7\% \pm 1.3\%$. It consisted of 88-96% Ca-Mg-montmorillonite.

3.5.1 Visual examination

Three bentonite blocks identified as BS-24-2, BS-24-3 and SH-SD1-01 (see [Figures 27, 28 and 62](#)) were studied, although the latter identification refers to the sensor contained in said block. [Figures 27 and 28](#) also indicate the location of the bentonite blocks in the FEBEX experiment.

Bentonites ref. BS-24-2 and BS-24-3 were not significantly different to the naked eye insofar as colour, degree of compaction, etc. However, these bentonites differed from that with reference SH-SD1-01, [Figure 129](#), which had a much higher degree of humidity. In this latter block (see [Figure 62](#)), diffusion of green and red corrosion products proceeding from corrosion of the metal sensor was observed.

In order to assess the differences observed in the bentonite and to explain some of the corrosion phenomena observed with the metal components, samples of the bentonite were characterised chemically and microbiologically, with the degree of humidity of the samples being determined on reception.

3.5.2 Determination of the humidity content

The humidity content of the bentonite was determined by heating the samples in an oven at 115

°C, until constant weight was achieved. The humidity loss of the three samples is shown in Table 3.

3.5.3 Chemical characterisation of bentonites

Chemical characterisation of the bentonite was carried out using two analytical processes:

1. Semi-quantitative microanalysis using EDS (Energy Dispersive Spectroscopy) of dry samples of bentonite.
2. Chemical analysis of the leached obtained in order to quantitatively assess the presence of certain ionic species in the sample.

EDS analysis of dry samples of bentonite

Figures 130, 131 and 132 show the EDS spectra obtained for bentonites ref. BS24-2, and SH-SD1-01. The bentonite sample of block SH-SD1-01 was obtained far from the zone of diffusion of the corrosion products proceeding from the sensor. The three analyses detected elements typical of bentonite, such as silicon, aluminium, magnesium and calcium, in similar percentage. Analysis of bentonite sample SH-SD1-01, taken from a zone with diffusion of reddish corrosion products, showed, as well as the above-mentioned elements, a significant percentage of iron, Figure 131. When the sample analysed was that taken from a zone close to the sensor, with the diffusion of greenish corrosion products, a significant peak of chrome and some sulphur was detected in addition to the iron, Figure 132.

Chemical analysis of the leached

Bentonite samples Ref. SH-SD1-01 and BS24-2 were leached using deionised water. The leachate obtained was analysed using spectrometry and ion chromatog-

raphy techniques. The results are shown in Table 4. The SH-SD1-01 bentonite analysed corresponds to a zone in which no diffusion of corrosion products was observed.

PH: Method EPA 9045 B pH for ground and wastes

Sulphides: Pre-treatment of the sample as per EPA 9030-A standard and determination of sulphides by evaluation, S.M. 4500

Conductivity: After aqueous leaching as per the electrometric method, S.M. 2510-B.

Chlorides, sulphates and nitrates: these were defined after aqueous leaching by means of ion chromatography, S.M. 4110-C.

3.5.4 Microbiological characterisation of the bentonite

The determination of the presence of aerobic and anaerobic bacteria was carried out by microbiological count, after extraction with phosphate buffer. The determination of the presence of sulphate-reducing bacteria, iron-oxidizing and sulphur-oxidizing bacteria, was carried out by the MPN (most probable number) method. Three bentonite samples were analysed:

Sample of bentonite from the block containing sensor SH-SD1-01. The sample was extracted from the zone in direct contact with the perforated sensor in the corrosion products diffusion zone.

Sample of bentonite extracted from the remains of the bentonite + corrosion products, adhered to the surface of sensor SH-SD1-01, in the zone closest to the Liner.

Sample of bentonite from block BS-24-2.

The results are shown in Table 5.

Table 3
Humidity content of bentonite samples.

Bentonite ref.	% weight loss
BS24-2	13.1
BS24-3	13.4
SH-SD1-01	21.5

Table 4
Chemical analysis of the leachate from the bentonites.

Parameter	Bentonite ref. SH-SD1-01	Bentonite ref. BS24-2
Sulphurs (%)	<0.005	<0.005
Sulphates (%)	0.05	
Chlorides (%)	0.03	
Nitrates (%)	<0.001	
pH	6.98	7.97
Conductivity ($\mu\text{S}/\text{cm}$)	309	—

Table 5
Microbiological characterisation of three samples of bentonite.

Microbe group	c.f.u./g count of sample		
	Bentonite ref. SH-SD1-01 Rock	Bentonite ref. SH-SD1-01 Liner	Bentonite ref. BS24-2
Anaerobic bacteria	0	0	0
Aerobic bacteria	2×10^2 (*)	4.23×10^3 (*)	0
Sulphate-reducing	1.08×10^2	3.77×10^2	0
Iron-oxidizing	0	0	—
Sulphur-oxidizing	0	0	—

(*) The whole count consisted of fungi.
c.f.u. : Colony forming unit

Component: Heater



Figure 1: Macrograph on reception.



Figure 2: Macrograph on reception.



Figure 3: Macrograph on reception.



Figure 4: Macrograph on reception.



Figure 5: Macrograph on reception.



Figure 6: Macrograph on reception.



Figure 7: Macrograph showing cut pieces of lid + cylinder.



Figure 8: Macrograph showing detail of lid + cylinder cut.

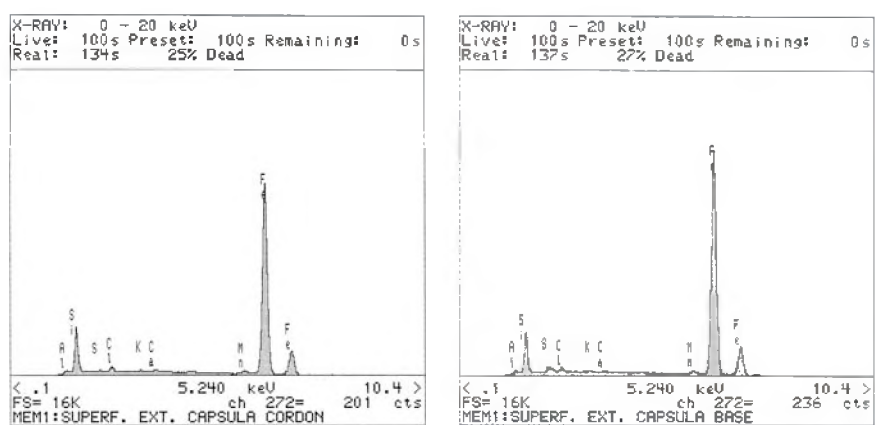


Figure 9: EDS spectra of a) the surface of the welded joint and b) cylinder.

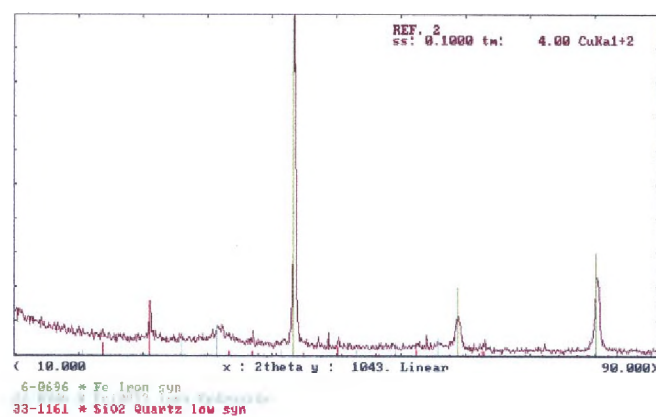


Figure 10: XRD spectrum of the cylinder surface.

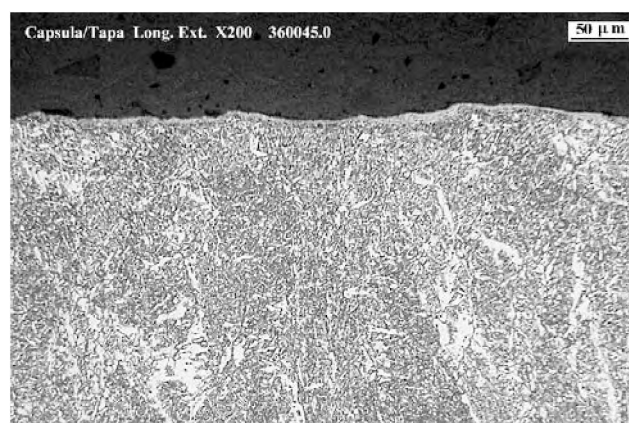


Figure 11: External surface of the welded joint.



Figure 12: Macrograph of the lid-cylinder welded joint test piece.

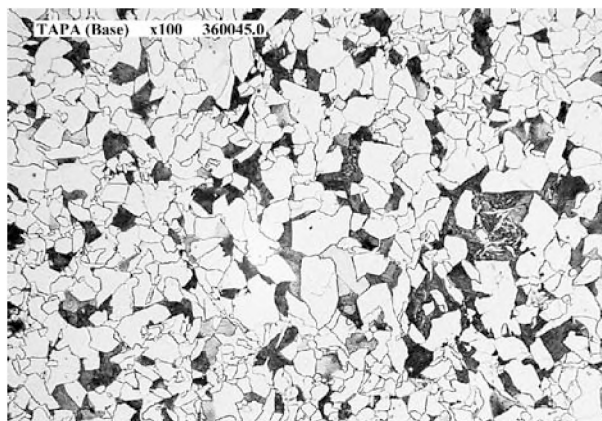


Figure 13: Optical micrograph of the lid structure (Unaffected base metal).

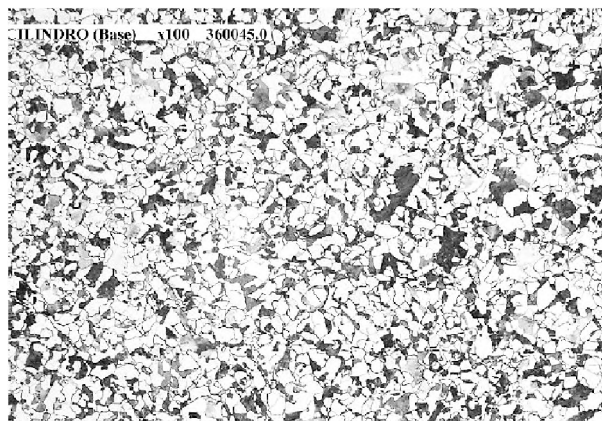


Figure 14: Optical micrograph of cylinder microstructure (Unaffected base metal).

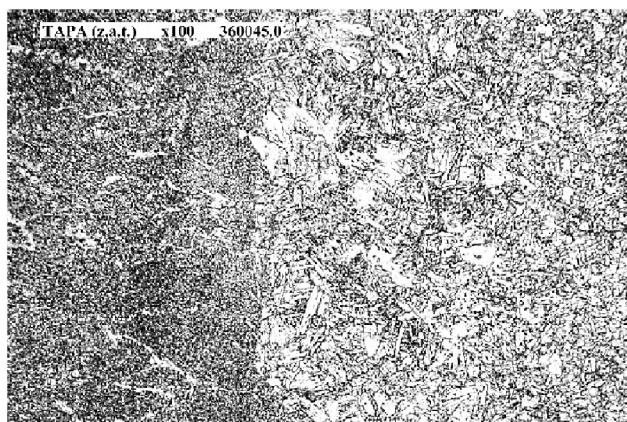


Figure 15: Optical micrograph of the HAZ in the lid joint.

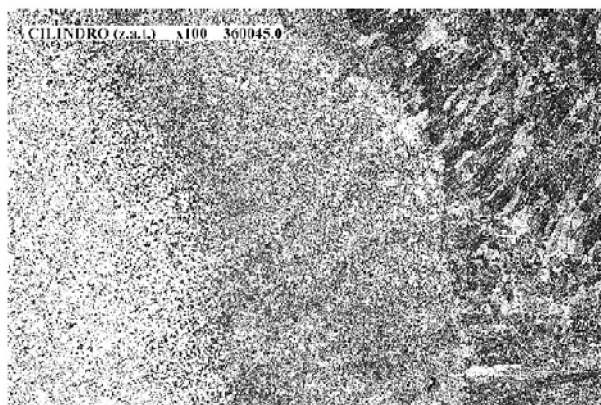


Figure 16: Optical micrograph of the HAZ in the cylinder joint.

Component: Liner

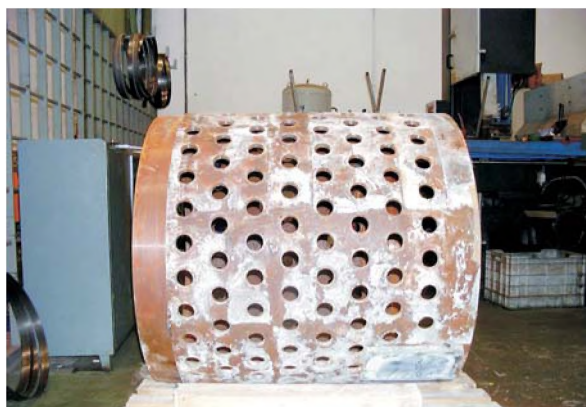


Figure 17: Liner segment studied.



Figure 18: Internal surface (G1 lower generatrix).



Figure 19: External surface (GS upper generatrix).



Figure 20: Detail of the external surface.

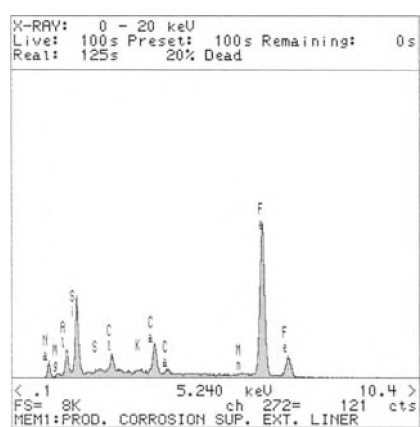


Figure 21: EDS spectrum of corrosion products on the external surface of the Liner.

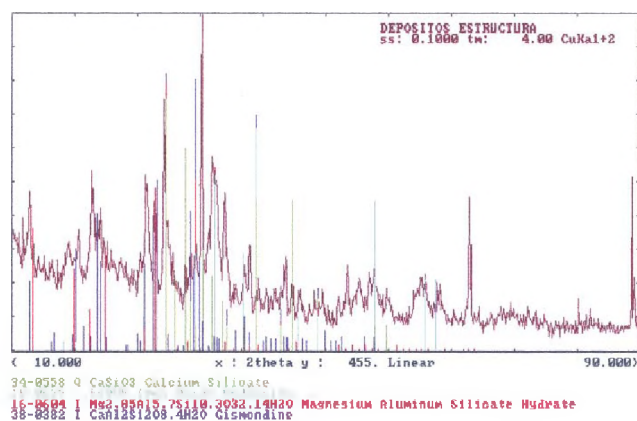


Figure 22: XRD spectrum of corrosion products on the external surface of the Liner.

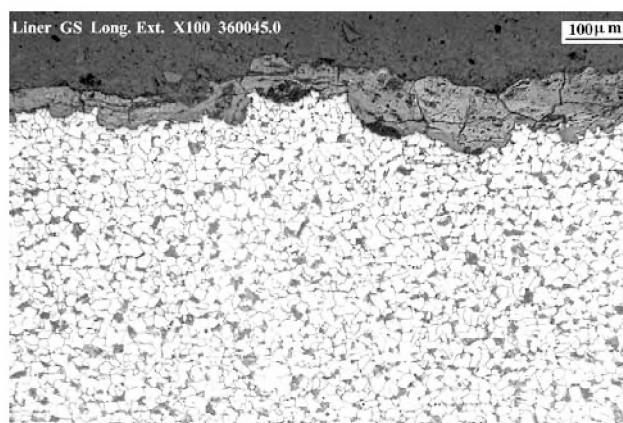


Figure 23: External surface of the upper generatrix liner.

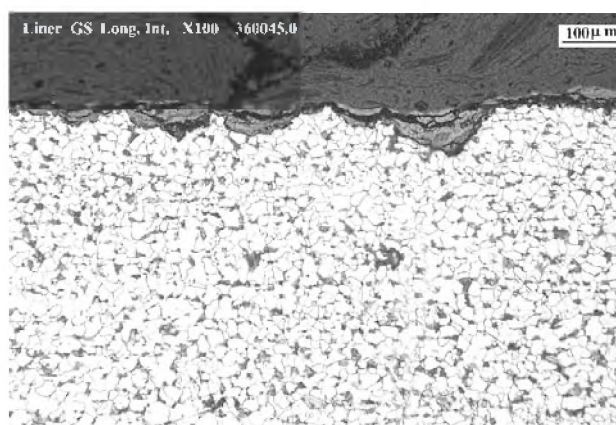


Figure 24: Internal surface of the upper generatrix liner.

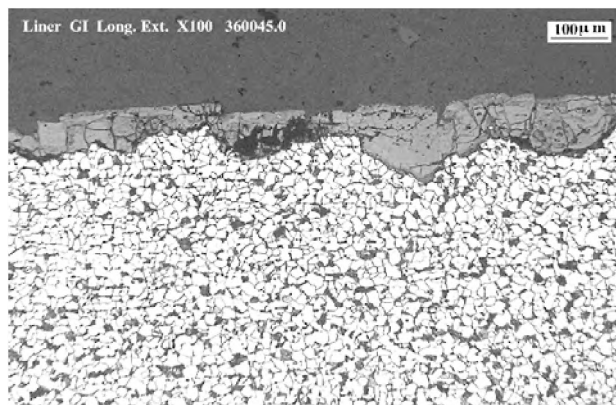


Figure 25: External surface of the lower generatrix liner.

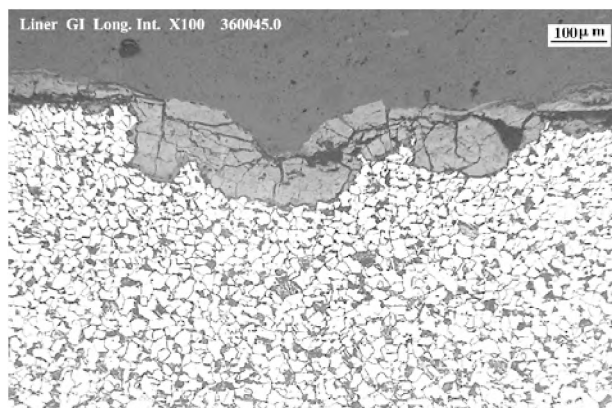


Figure 26: Internal surface of the lower generatrix liner.

Component: Corrosion coupons

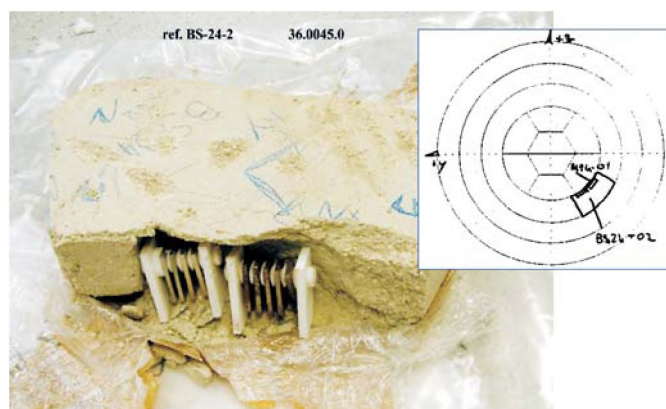


Figure 27: Macrograph of the bentonite block Ref. BS-24-2 and diagram of its location in the FEBEX experiment.

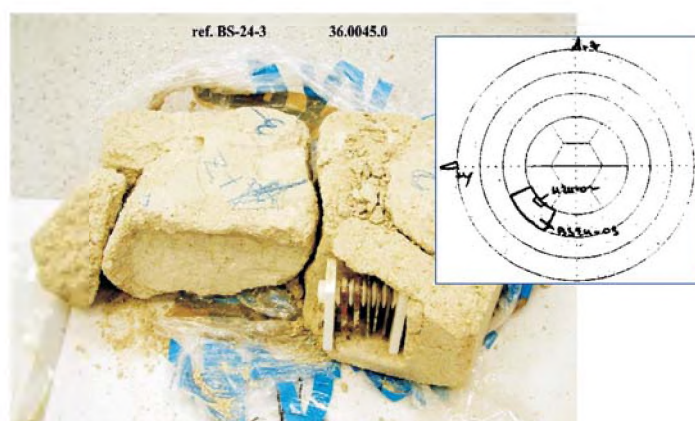


Figure 28: Macrograph of the bentonite block Ref. BS-24-3 and diagram of its location in the FEBEX experiment.



Figure 29: Macrograph on receipt.



Figure 30: Macrograph of bentonite blocks on receipt.

Component: Corrosion coupons: Rack R1C (TStE355)

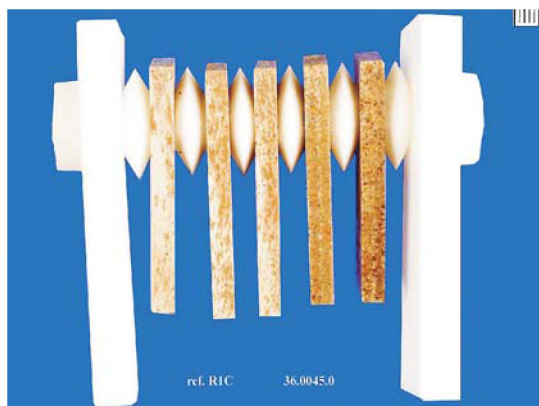


Figure 31: Reception rack ref. R1C (TStE355 steel).

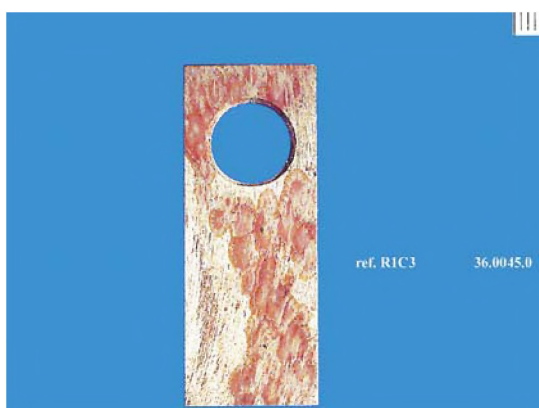


Figure 32: Corrosion coupon Ref. R1C3.

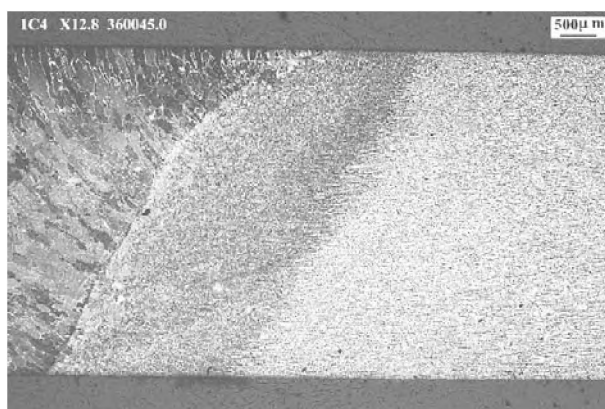


Figure 33: FCAW welded joint, coupon Ref. R1C4.



Figure 34: Base material, coupon Ref. R1C4.

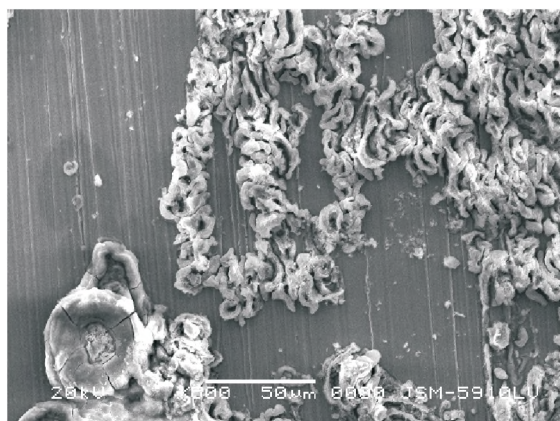


Figure 35: SEM micrograph of the surface of coupon Ref. R1C3.

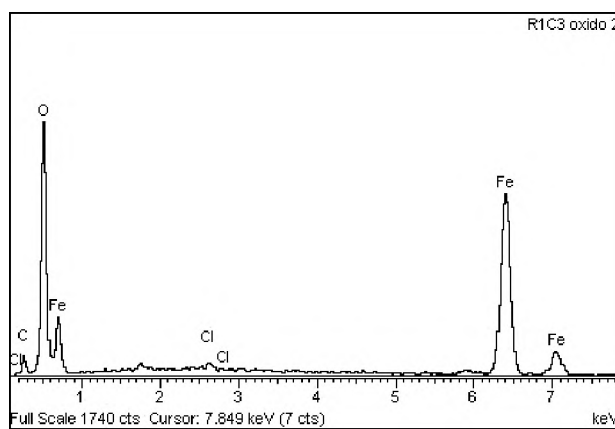


Figure 36: EDS spectrum of corrosion products on the surface of coupon Ref. R1C3.

Component: Corrosion coupons: Rack R2C (AISI 316L).

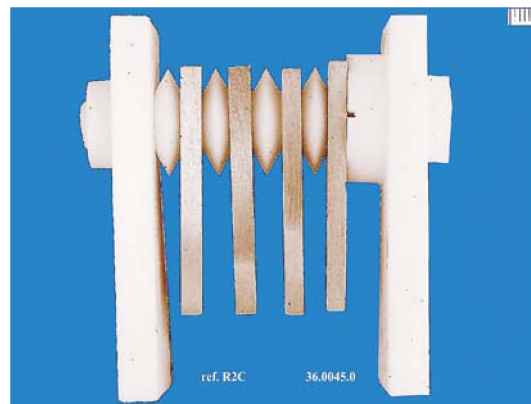


Figure 37: Reception rack Ref. R2C (316L steel).

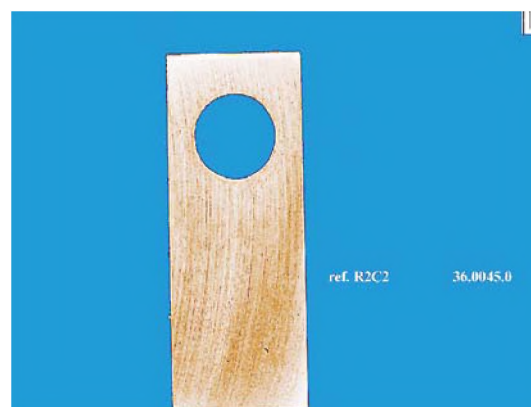


Figure 38: Corrosion coupon Ref. R2C2.

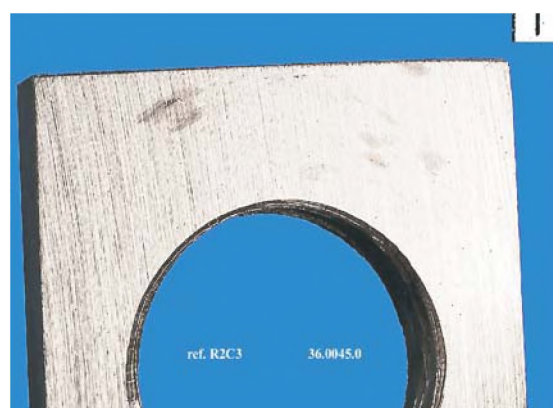


Figure 39: Corrosion coupon Ref. R2C3.

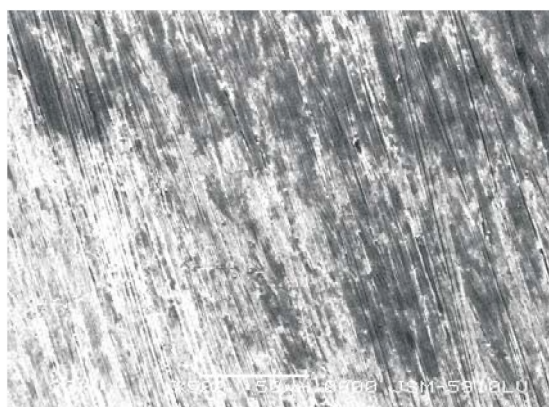


Figure 40: SEM micrograph of surface of R2C3.

Component: Corrosion coupons: Rack R3C (Titaniums)



Figure 41: Reception rack ref. R3C (titaniums).



Figure 42: Corrosion coupon Ref. R3C2 (Ti Gr-2).



Figure 43: Corrosion coupon Ref. R3C3 (Ti 6r-7).

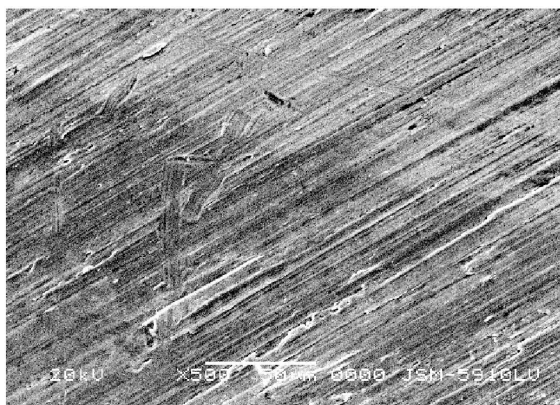


Figure 44: SEM micrograph of surface of R3C2 (Ti 6r-2).

Component: Corrosion coupons: Rack R4C (Coppers)

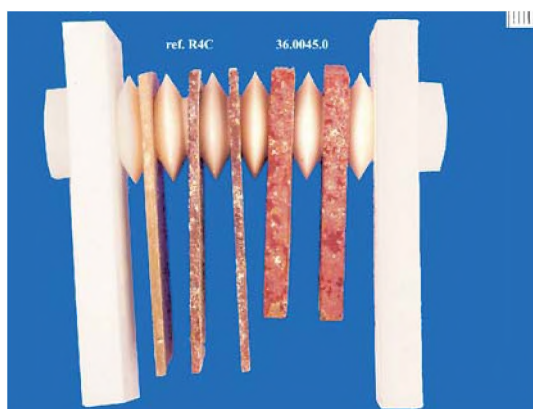


Figure 45: Reception rack ref. R4C (coppers).

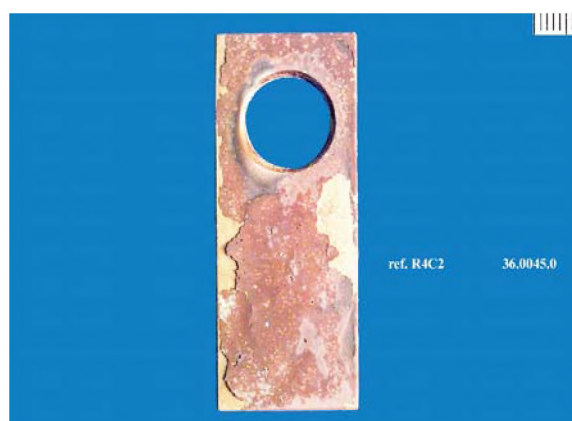


Figure 46: Corrosion coupon Ref. R4C2 (Cu-ETP).

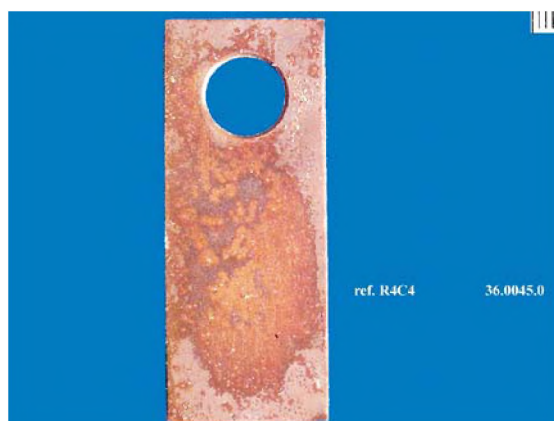


Figure 47: Corrosion coupon Ref. R4C4 (Cu10Ni).

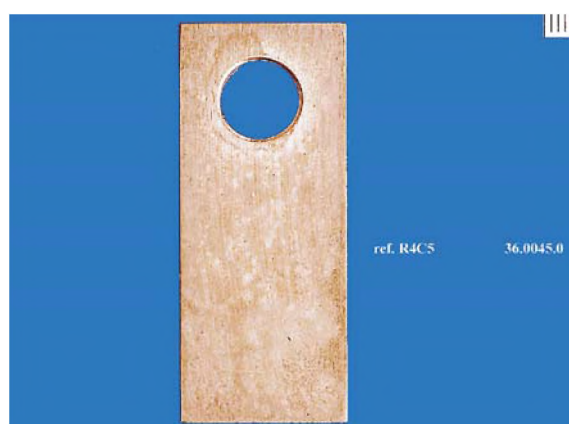


Figure 48: Corrosion coupon Ref. R4C5 (Cu30Ni).

Component: Corrosion coupons: Rack R4C (Coppers)

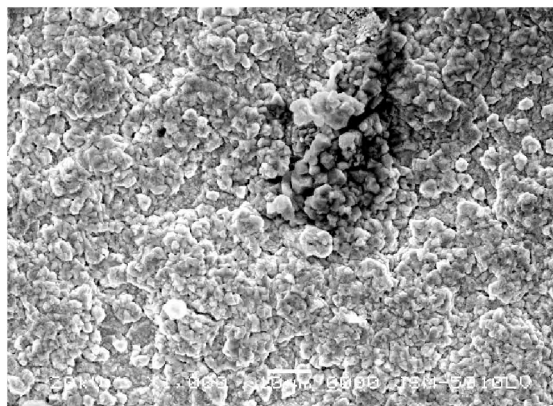


Figure 49: SEM micrograph of the surface of Ref. R4C2 (Cu-ETP).

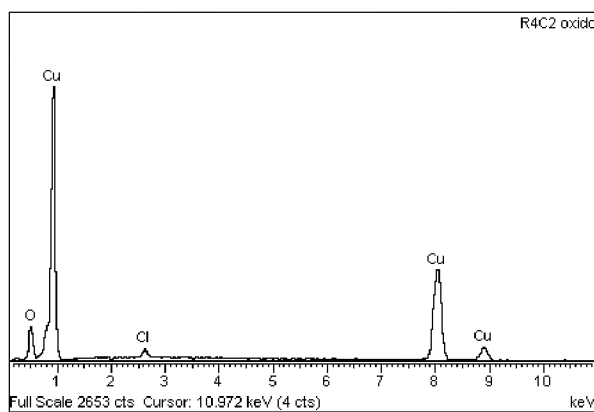


Figure 50: EDS of corrosion products of Ref. R4C2.

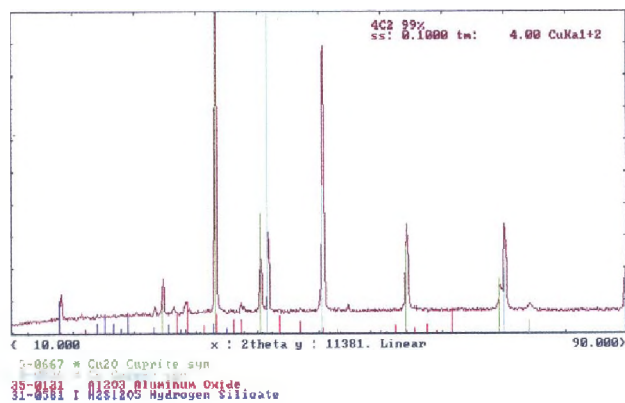


Figure 51: XRD spectrum of corrosion products of Ref. R4C2.

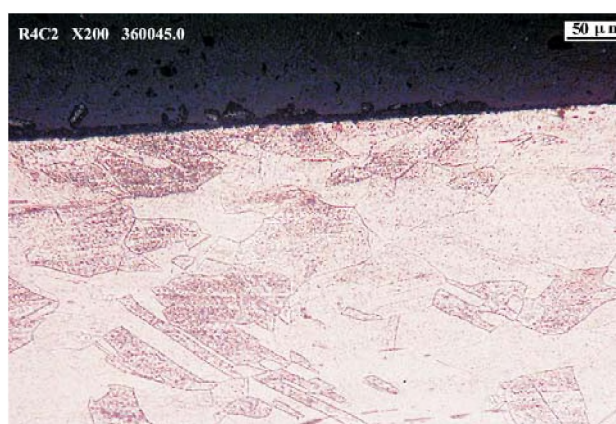


Figure 52: Corrosion coupon Ref. R4C2.

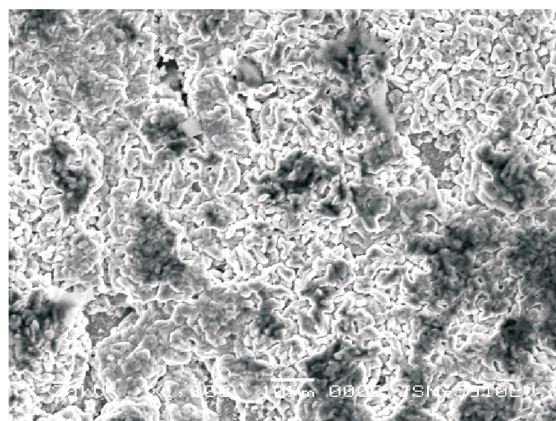


Figure 53: SEM micrograph of the surface of Ref. R4C4 (Cu10Ni).

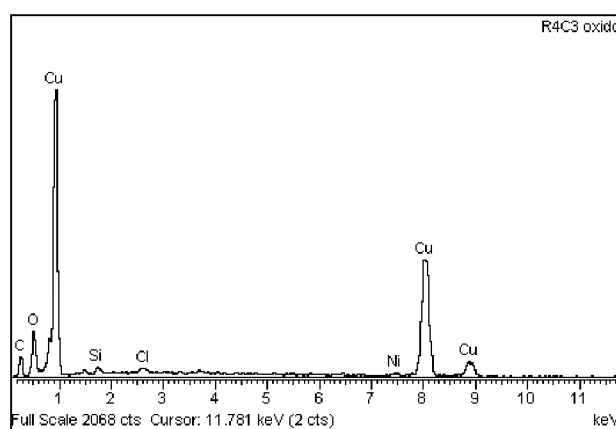


Figure 54: EDS spectrum of corrosion products of Ref. R4C4.

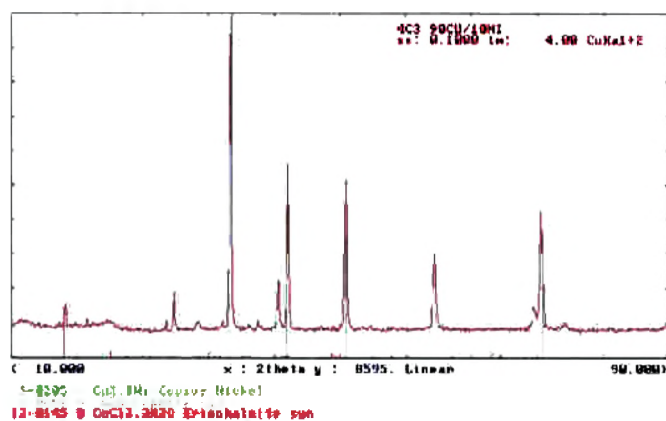


Figure 55: XRD spectrum of corrosion products of Ref. R4C4.

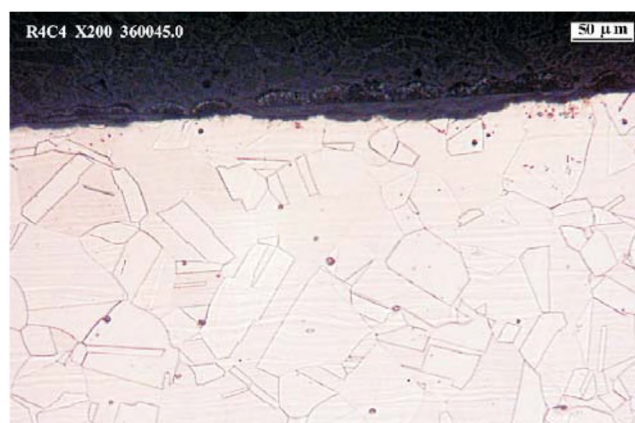


Figure 56: Corrosion coupon Ref. R4C4.

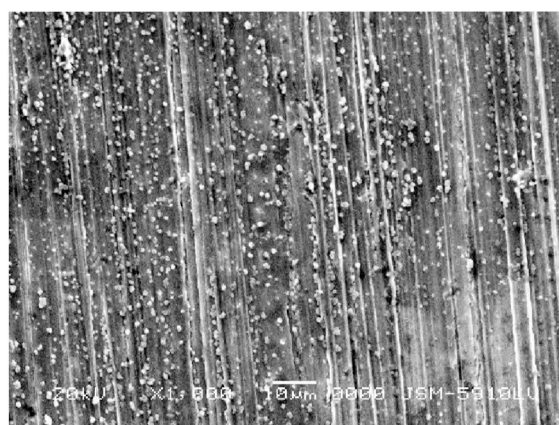


Figure 57: SEM micrograph, surface of Ref. R4C5 (Cu30Ni).

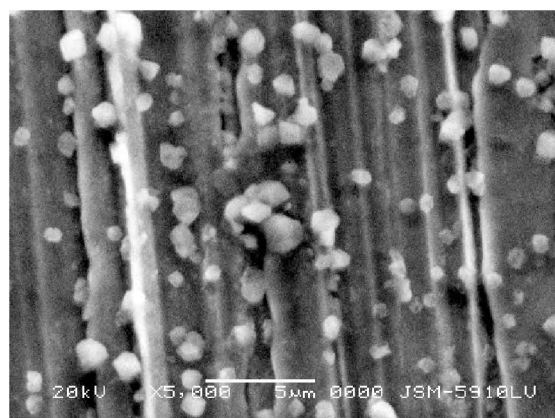


Figure 58: SEM micrograph, surface of Ref. R4C5 (Cu30Ni).

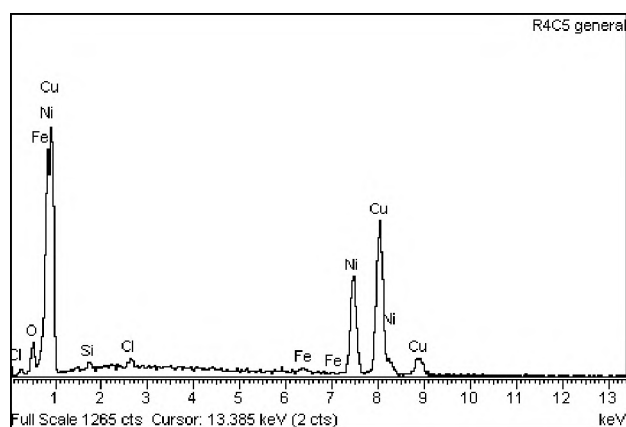


Figure 59: EDS spectrum of corrosion products of Ref. R4C5.

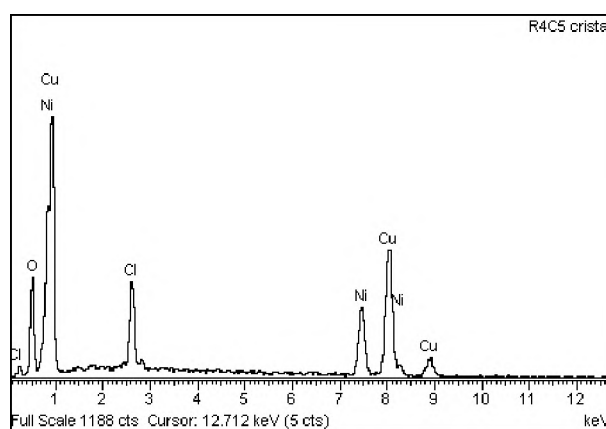


Figure 60: EDS spectrum of crystals, Ref. R4C5.

Component: Sensors: SH-SD1-01

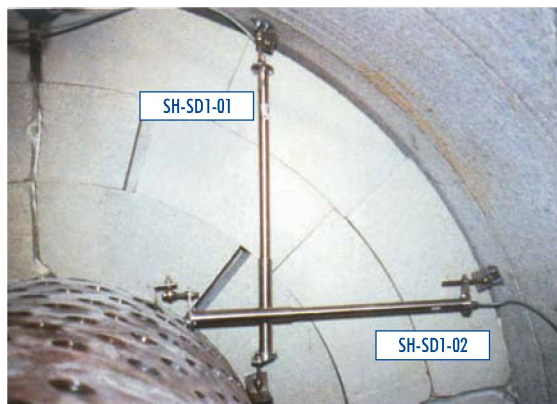


Figure 61: Extensometers – FEBEX test.



Figure 62: Reception of sensor SH-SD1-01 in block of bentonite.

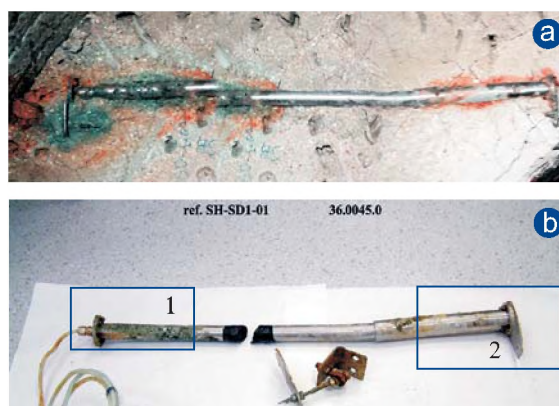


Figure 63: a) On-site (19/06/02), b) reception at INASMET.

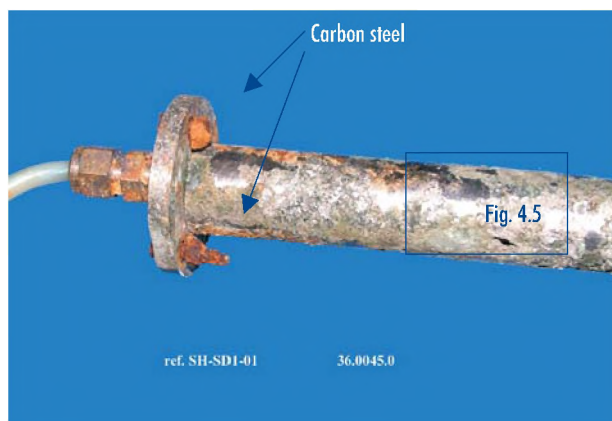


Figure 64: Detail of the sensor in zone 1, close to the rock.



Figure 65: Macrograph detail of 64.

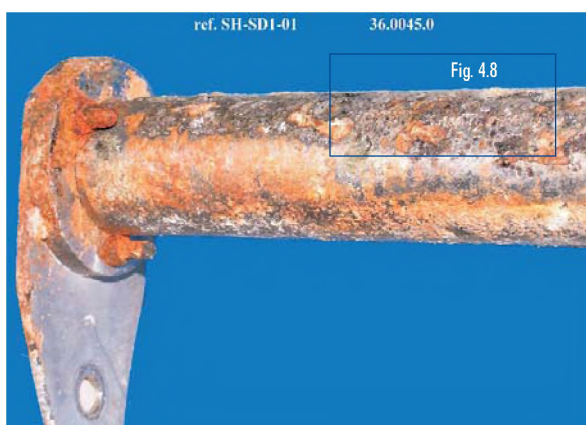


Figure 66: Detail of sensor in zone 2, close to the liner.

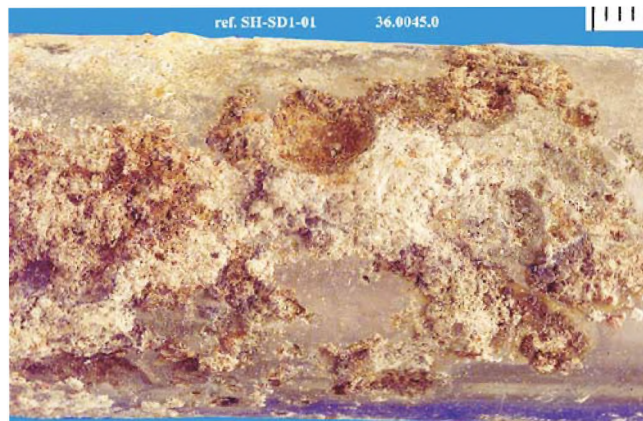


Figure 67: Macrograph detail of 66.

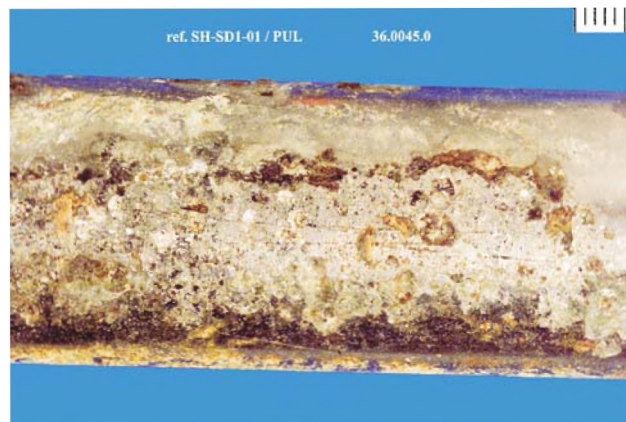


Figure 68: Macrograph detail of 66.



Figure 69: Detail of rock-sensor joint SH-SD1-01.



Figure 70: Detail of rock-sensor joint SH-SD1-01.

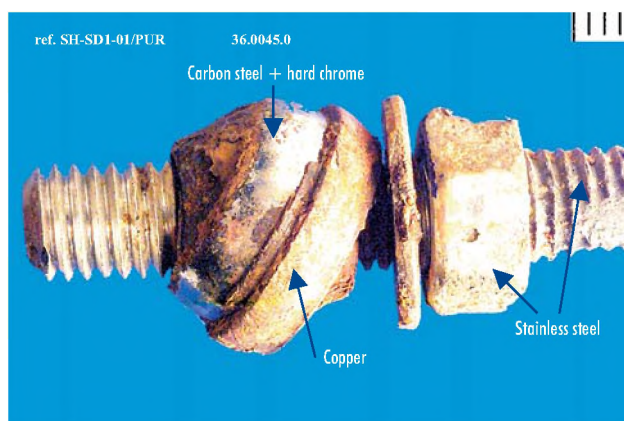


Figure 71: Detail of rock-sensor joint SH-SD1-01.



Figure 72: Detail of rock-sensor joint SH-SD1-01.

Component: Sensors: SH-SD1-02

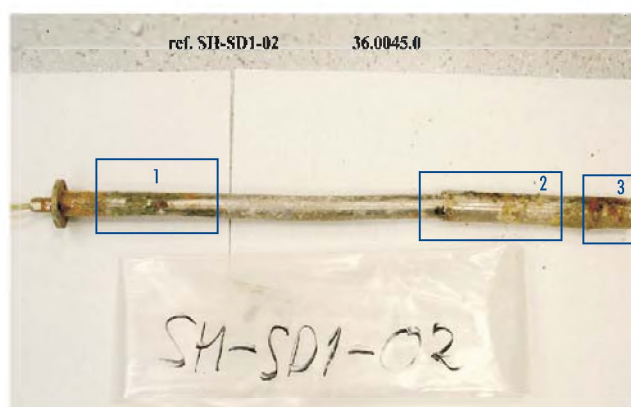


Figure 73: Reception of sensor SH-SD1-02.



Figure 74: Detail of sensor in zone 1, close to the rock.

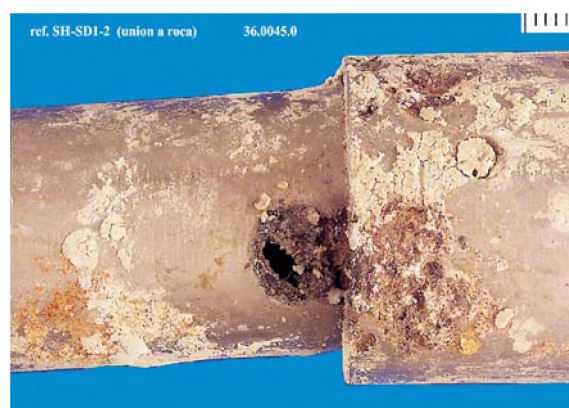


Figure 75: Detail of sensor in zone 3.

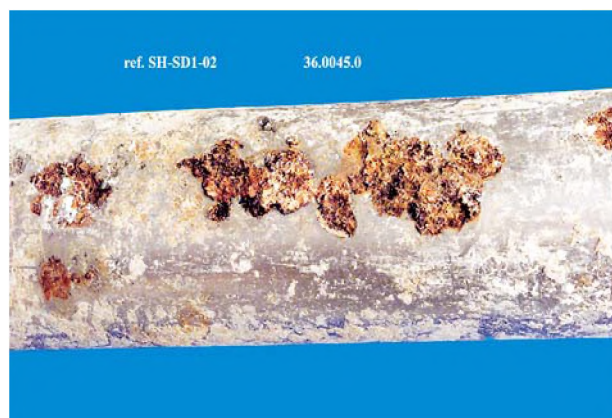


Figure 76: Detail of sensor in zone 3.

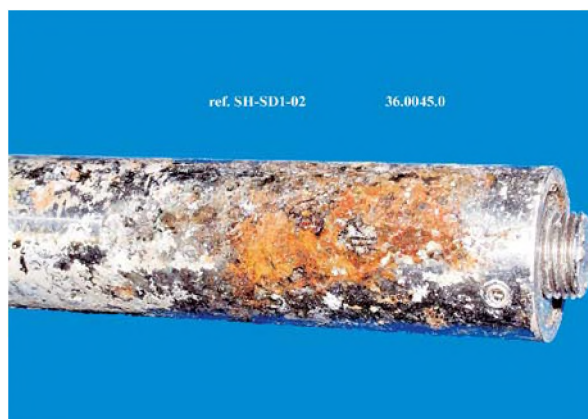


Figure 77: Detail of sensor in zone 3, close to the liner.



Figure 78: Detail of Figure 77.

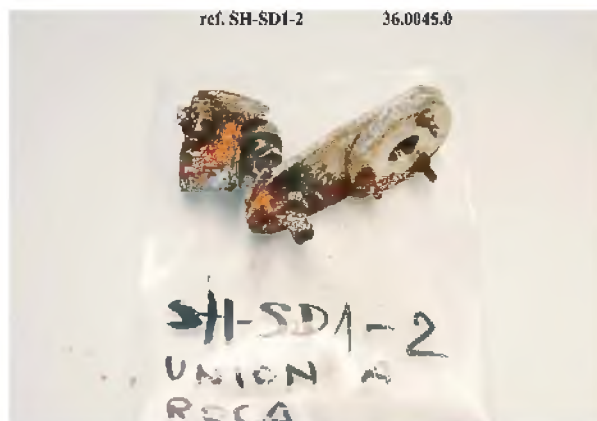


Figure 79: Detail of rock-sensor joint SH-SD1-02.



Figure 80: Detail of liner-sensor joint SH-SD1-02.



Figure 81: Detail of rock-sensor joint SH-SD1-02.



Figure 82: Detail of liner-sensor joint SH-SD1-02.

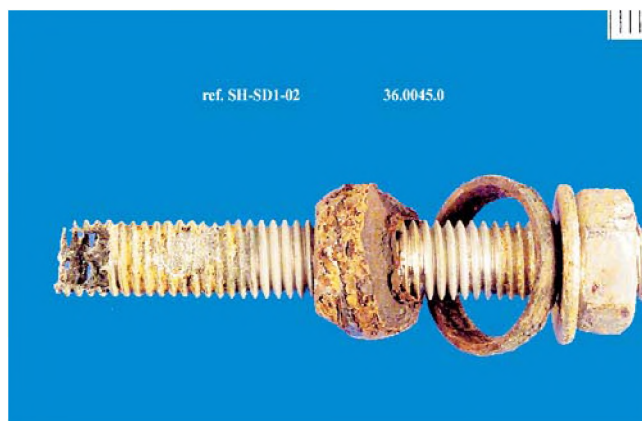


Figure 83: Detail of liner-sensor joint SH-SD1-01.

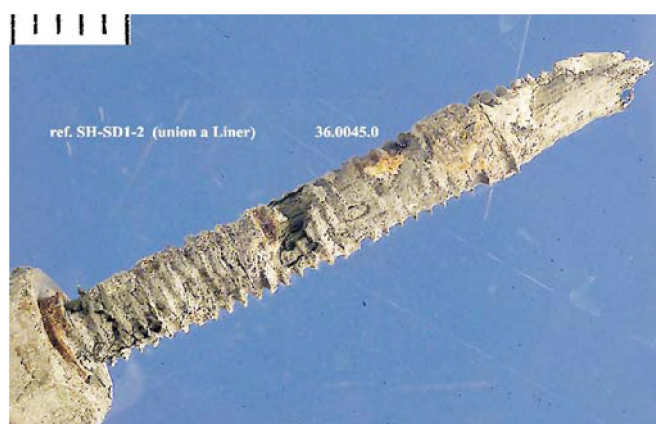


Figure 84: Detail of liner-sensor joint SH-SD1-01.

Component: Sensors: SH-SD1-01

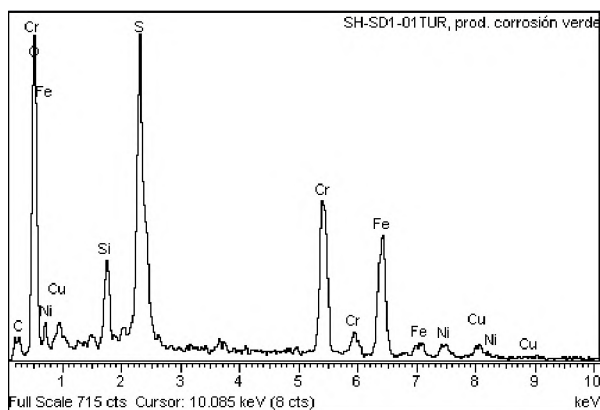


Figure 85: EDS spectrum of green corrosion products on sensor SH-SD1-01, close to the rock.

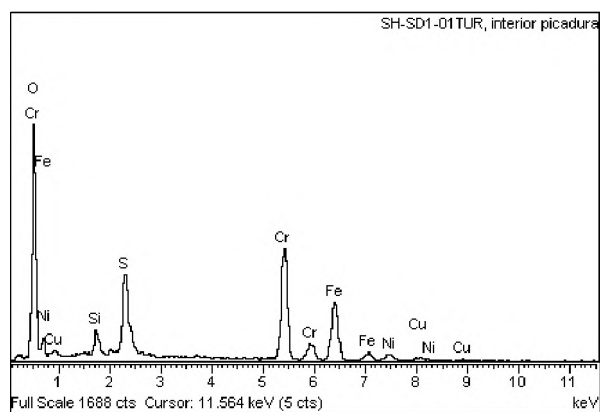


Figure 86: EDS spectrum of corrosion products inside the pitting on sensor SH-SD1-01, close to the rock.

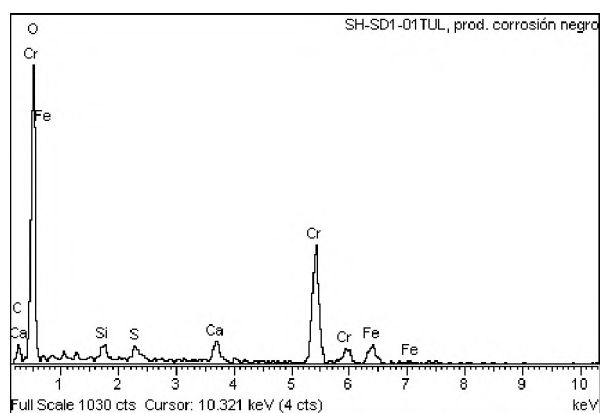


Figure 87: EDS spectrum of black corrosion products on sensor SH-SD1-01, close to the liner.

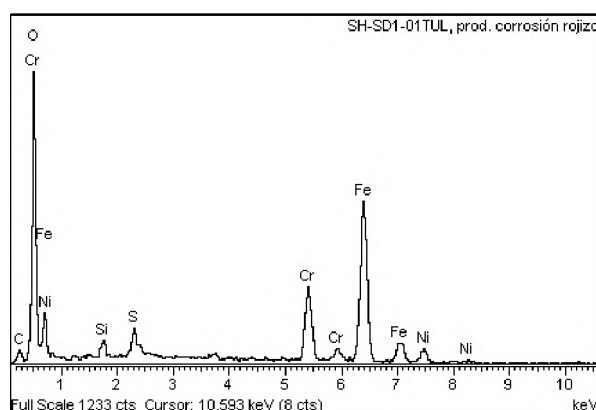


Figure 88: EDS spectrum of red corrosion products on sensor SH-SD1-01, close to the liner.

Component: Sensors: SH-SD1-02

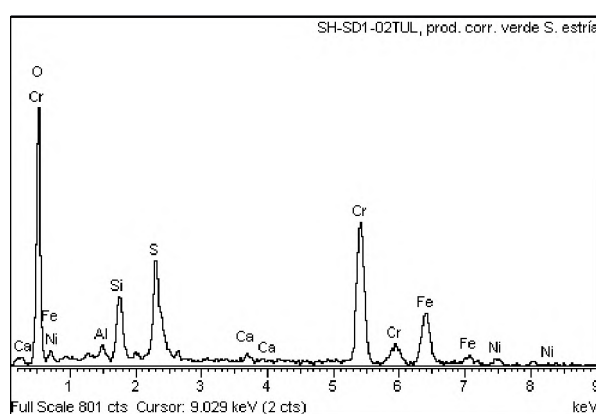


Figure 89: EDS spectrum of green corrosion products on sensor SH-SD1-02, close to the rock.

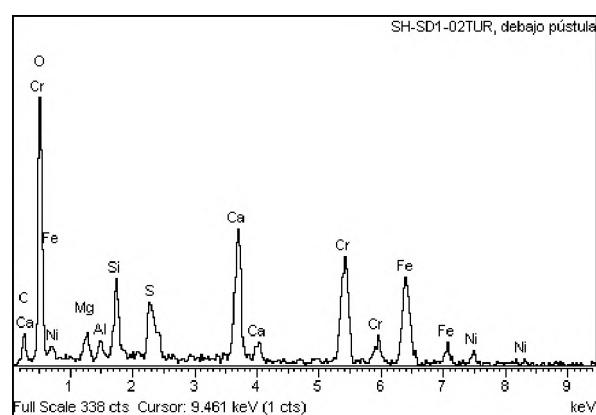


Figure 90: EDS spectrum of corrosion products/deposits under pustules on sensor SH-SD1-02, close to the liner.

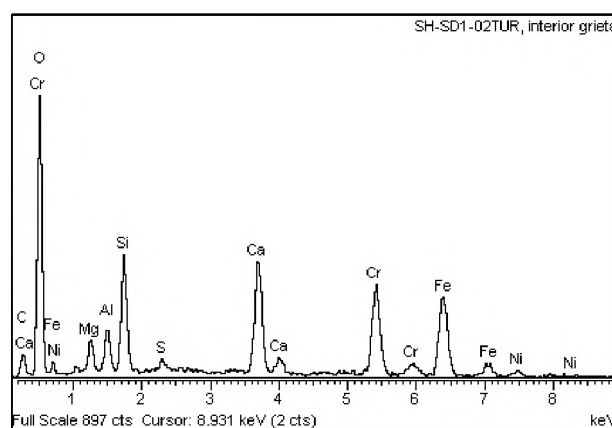


Figure 91: EDS spectrum of corrosion products inside crack on sensor SH-SD1-02, close to the liner.

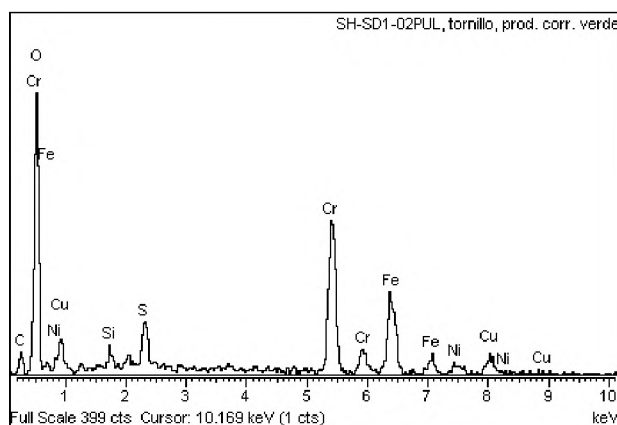


Figure 92: EDS spectrum of green corrosion products on the screw fixing sensor SH-SD1-02 to the liner.

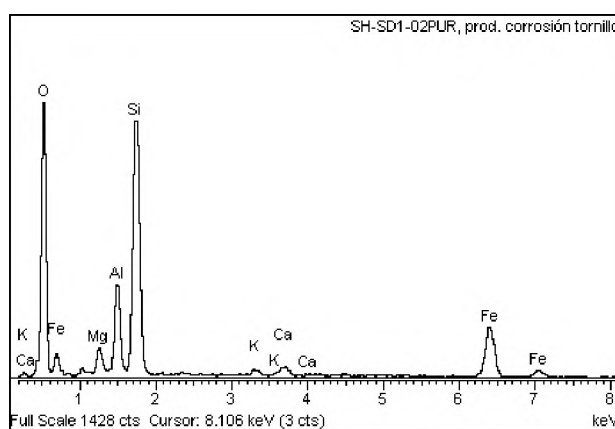


Figure 93: EDS spectrum of red corrosion products on the plate fixing sensor SH-SD1-02 to the rock.

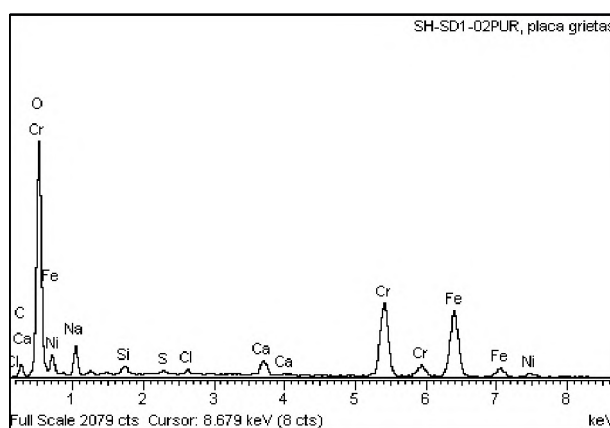


Figure 94: EDS spectrum inside crack on the plate fixing sensor SH-SD1-02 to the rock.

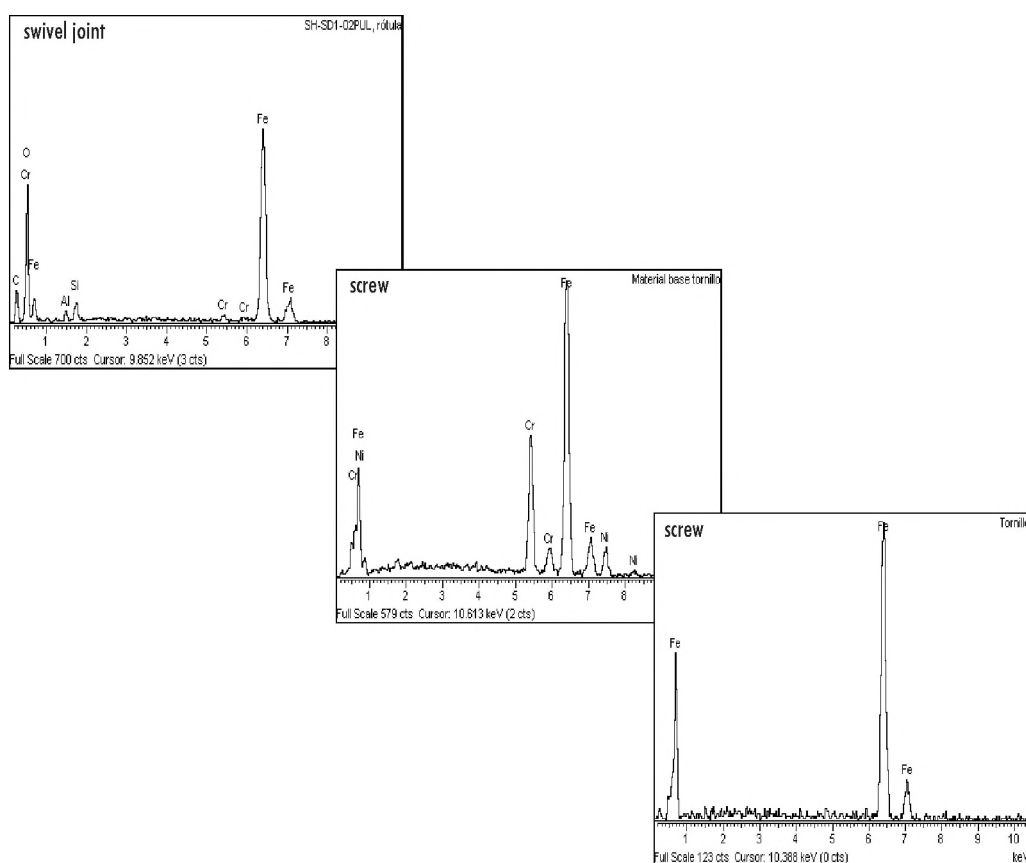


Figure 95: EDS spectra of the swivel joint and screw (austenitic) of the liner fixing plate, and of the screw fixing the sensor to the plate (Figure 64) Component: Sensors: SH-SD1-01.

Component: Sensors: SH-SD1-01

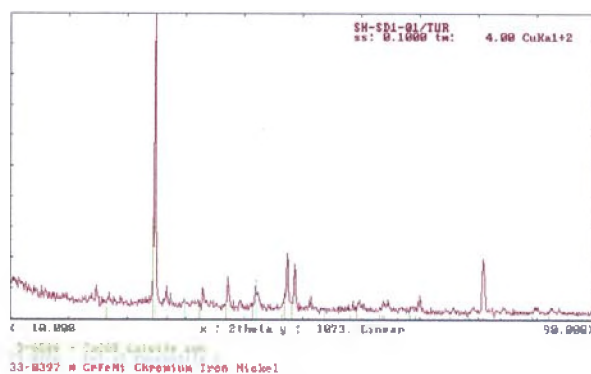


Figure 96: XRD spectrum of green corrosion products on sensor SH-SD1-01, close to the rock.

Component: Sensors: SH-SD1-02

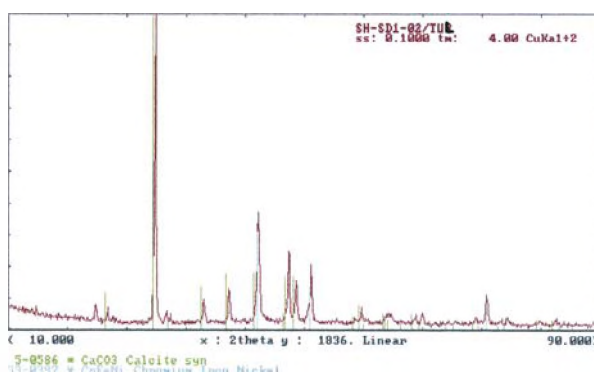


Figure 97: XRD spectrum of corrosion products on sensor SH-SD1-02, close to the liner.

Component: Sensors: SH-SD1-01

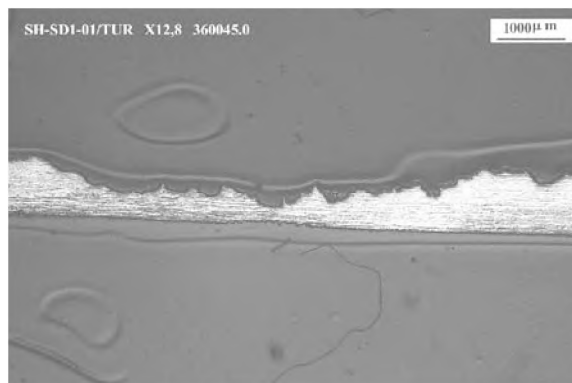


Figure 98: Longitudinal section, zone 1.



Figure 99: Detail of Figure 98.

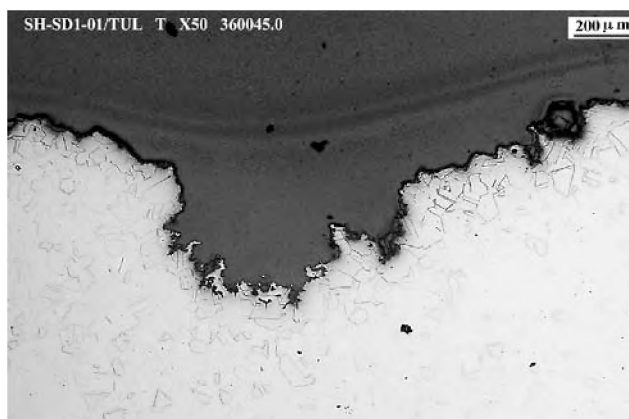


Figure 100: Transversal section, zone 2.



Figure 101: Detail of Figure 100.

Component: Sensors: SH-SD1-02

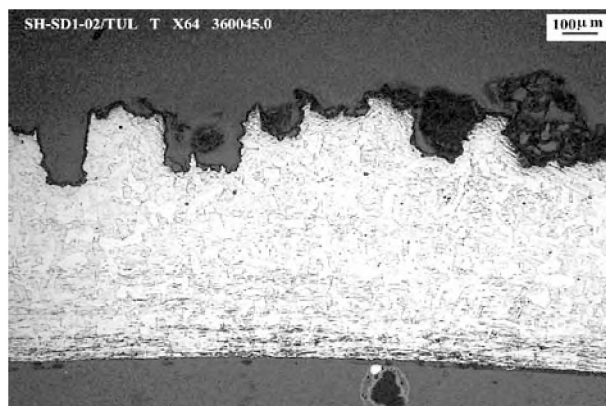


Figure 102: Transversal section of sensor in zone 1.



Figure 103: Detail of Figure 102.

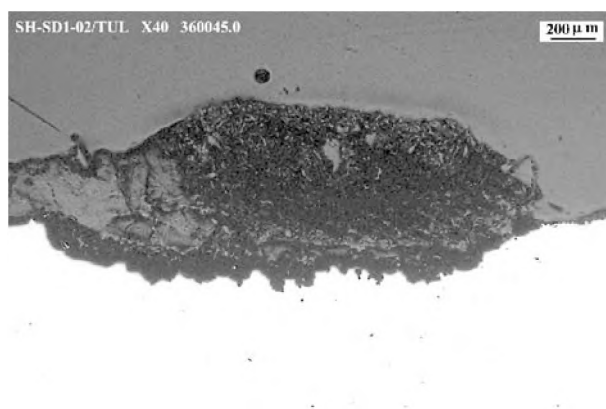


Figure 104 Transversal section of pustule in zone 2.



Figure 105: Figure 104, obtained using polarised light.

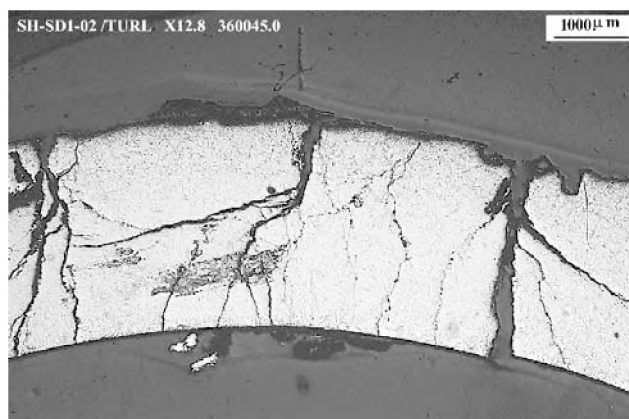


Figure 106: Transversal section of sensor SH-SD1-02 in zone 4.



Figure 107: Optical micrograph detail of Figure 106.

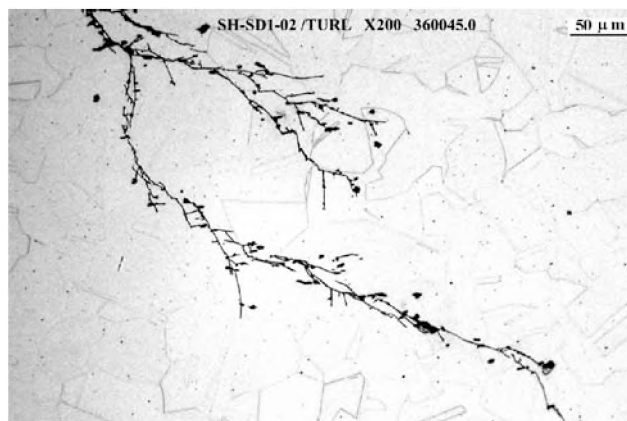


Figure 108: Detail of Figure 106.

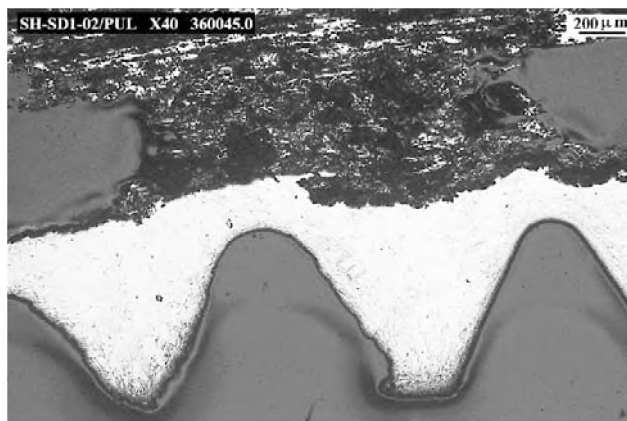


Figure 109: Longitudinal section of liner fixing screw.

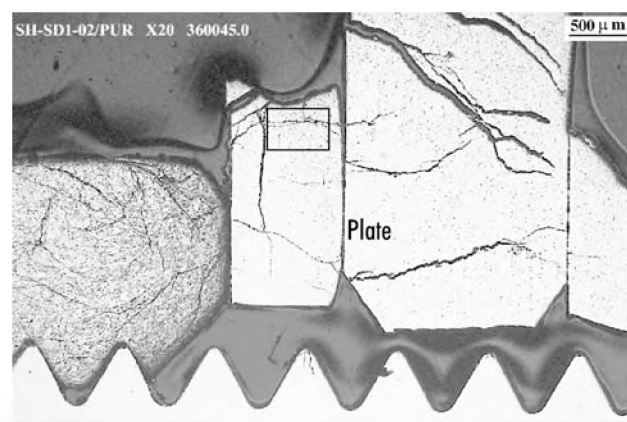


Figure 110: Cross-section of rock-sensor SH-SD1-02 fixing plate.

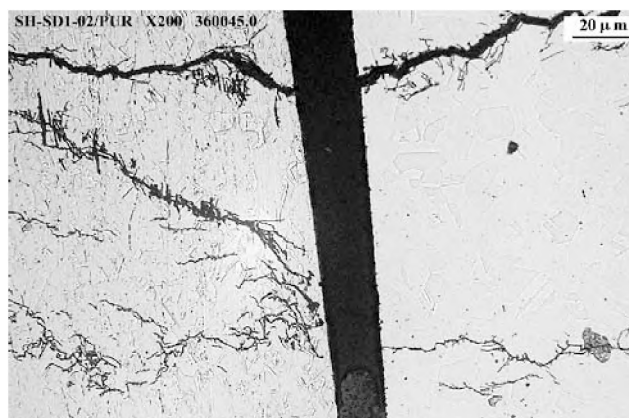


Figure 111: Detail of Figure 109.

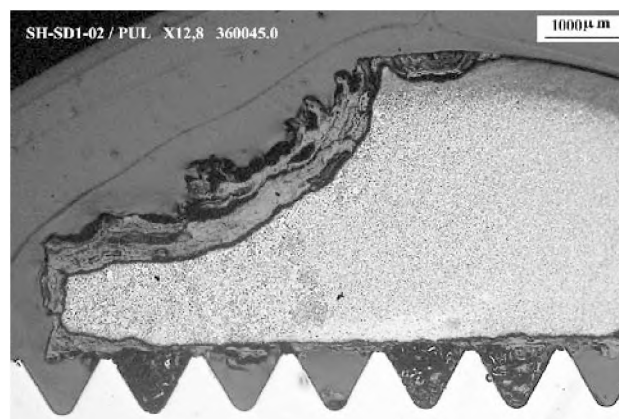


Figure 112: Cross-section of line-sensor SH-SD1-02 fixing.

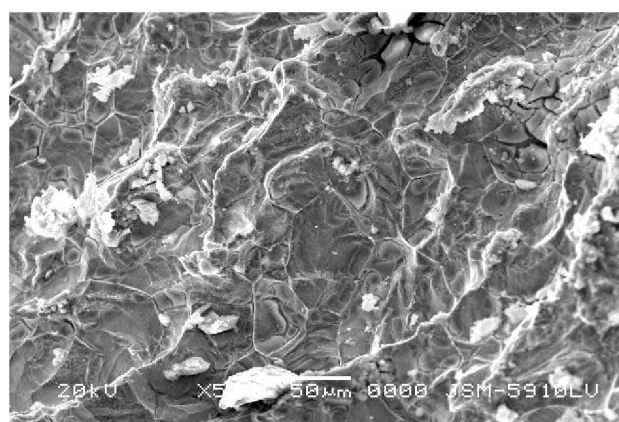


Figure 113: SEM of pitting in zone 2 of sensor SH-SD1-01.

Component: Sensors TSE1-2 and TSD1-11

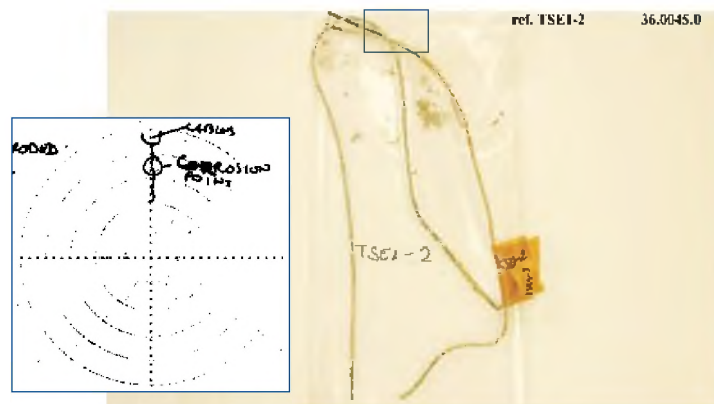


Figure 114: Reception of sensor TSE1-2 and location.

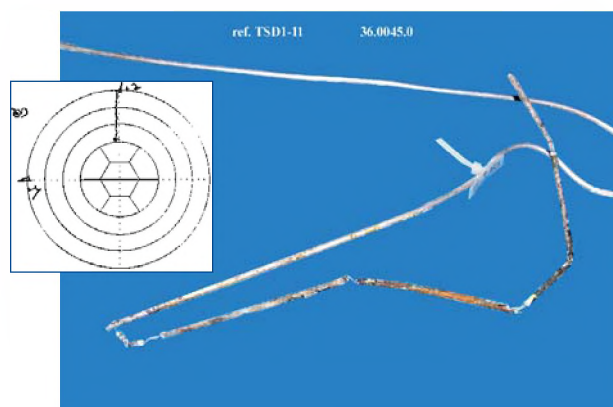


Figure 115: Reception of sensor TSD1-11 and location.



Figure 116: Detail of sensor TSE1-2.

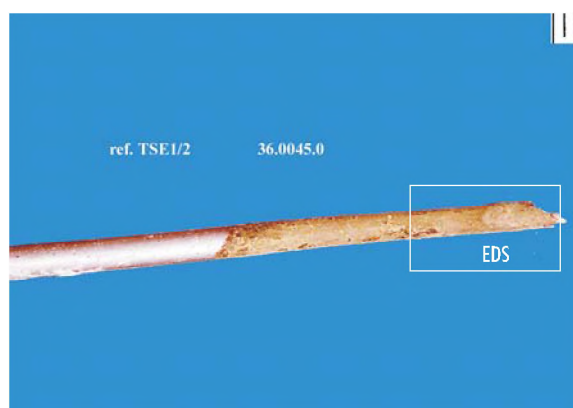


Figure 117: Detail of sensor TSE1-2.

Component: Sensors: ref. TSE1-2 and TSD1-11



Figure 118: Detail of sensor TSD1-11.



Figure 119: Detail of sensor TSD1-11.

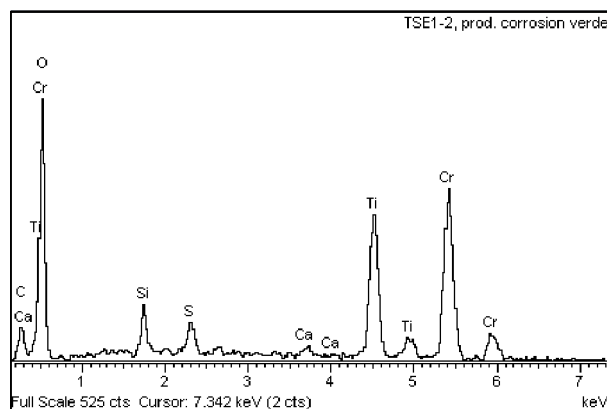


Figure 120: EDS spectrum of green corrosion products on thermocouple TSE1-2.

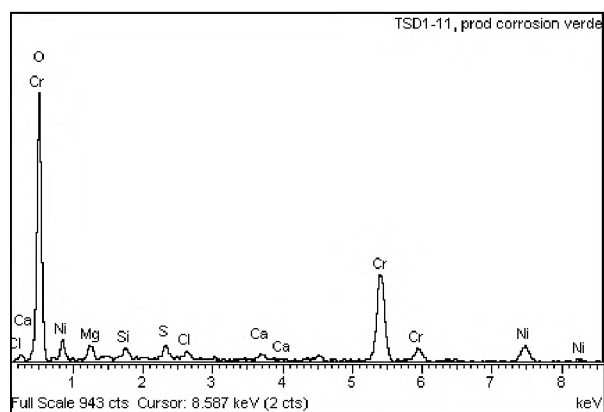


Figure 121: EDS spectrum of green corrosion products on thermocouple TSD1-11.

Component: Sensors TSE1-2 and TSD1-11

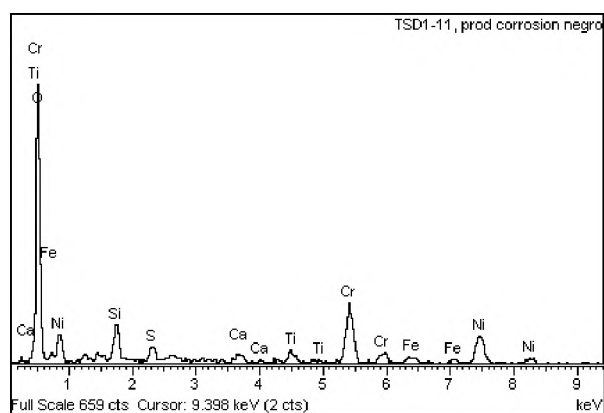


Figure 122: EDS spectrum of black corrosion products on thermocouple TSD1-11.

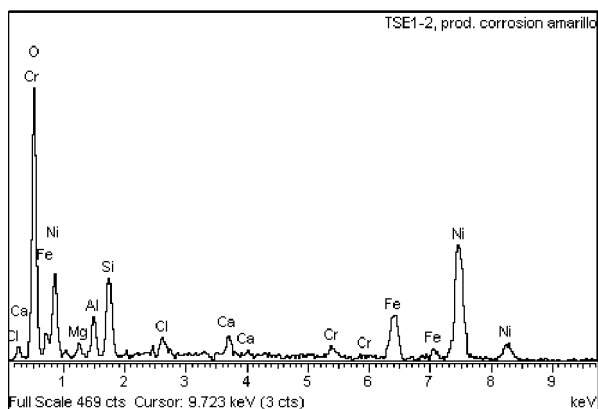


Figure 123: EDS spectrum of yellow corrosion products on thermocouple TSE1-2.

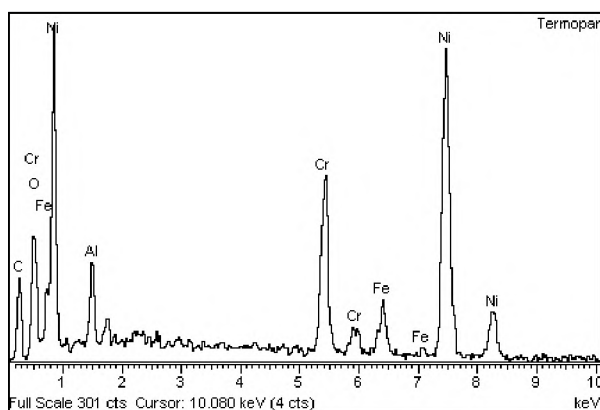


Figure 124: EDS spectrum of outer tube of thermocouple TSD1-11.

Component: Sensor ref. TSD1-11

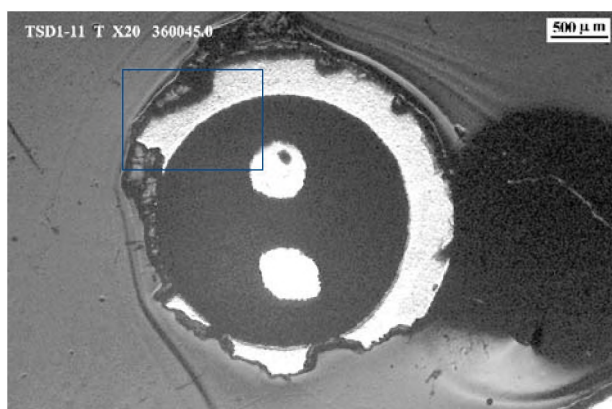


Figure 125: Transversal section of thermocouple TSD1-11.

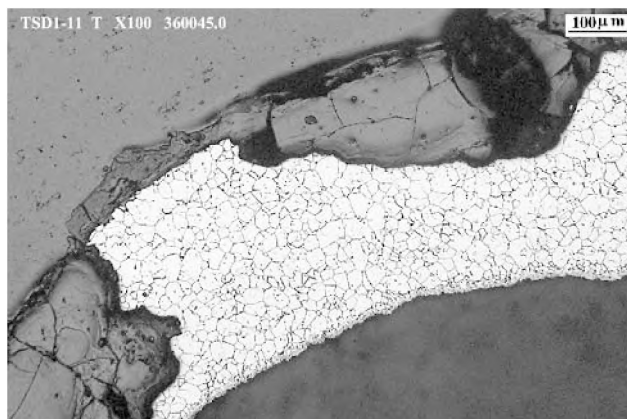


Figure 126: Detail of Figure 125.

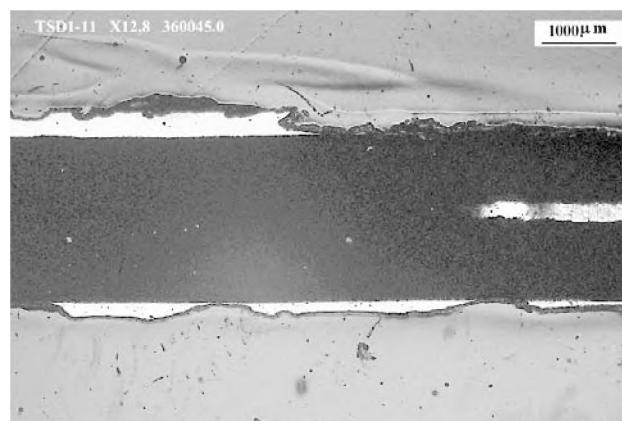


Figure 127: Longitudinal section of thermocouple TSD1-11.

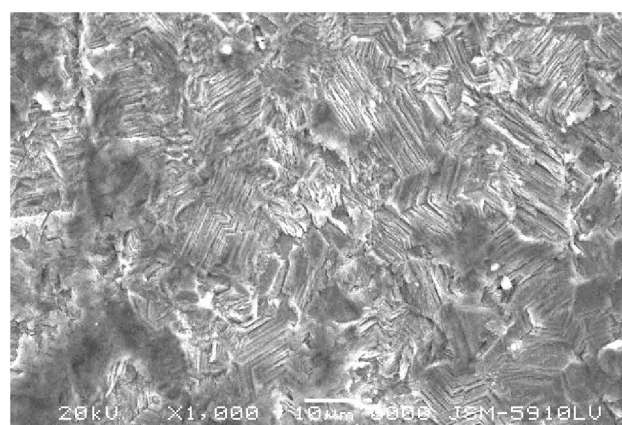


Figure 128: SEM of active surface on thermocouple TSD1-11.

Component: Sensors: SH-SD1-02



Figure 129: Samples from blocks BS-24-2 and SH-SD1-01.

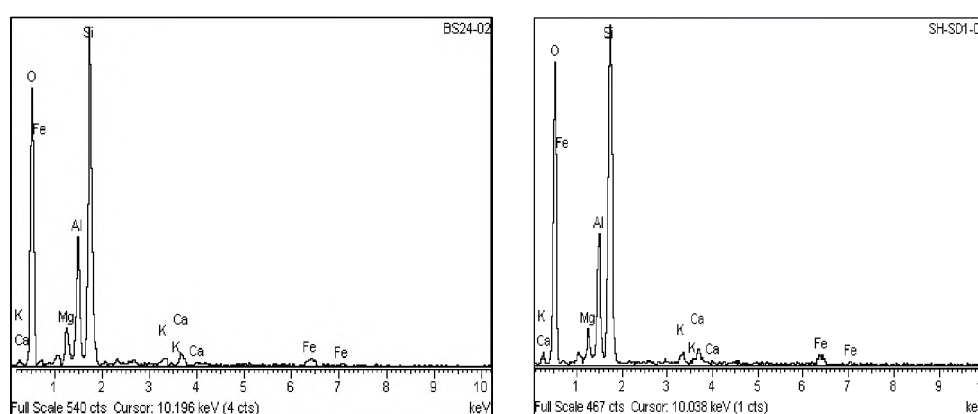


Figure 130: EDS spectra of samples Ref. BS24-02 and SH-SD1-01.

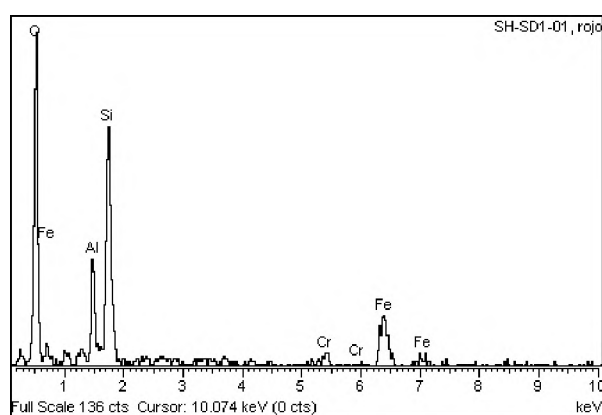


Figure 131: EDS spectrum of sample Ref. SH-SD1-01, in the zone of diffusion of reddish corrosion products.

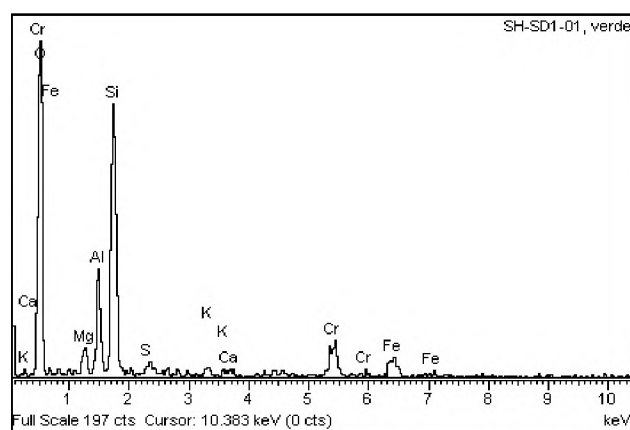


Figure 132: EDS spectrum of sample Ref. SH-SD1-01, in the zone of diffusion of greenish corrosion products.



4. Analysis of the results

4. Analysis of the results

The results obtained from the study carried out are commented on below:

Heater

The heater underwent very slight generalised corrosion. The almost complete absence of humidity around the heater as a result of heating, the evolution towards ever more anoxic conditions within the burial site, as well as the fact that it was not in direct contact with the bentonite, avoided or slowed down the progression of generalised corrosion, as well as the start and progression of other localised corrosion phenomena.

Liner

This element suffered generalised corrosion that did not advance uniformly, somewhat greater than that suffered by the heater. The test conditions of the guide tube, in direct contact with the bentonite and with a greater level of humidity in its surroundings, justify the difference in the extent of the generalised corrosion.

Corrosion coupons

The carbon steel coupons showed very slight generalised corrosion, with corrosion rates values of $0.10 \mu\text{m}/\text{year}$. These values are significantly lower than those obtained from laboratory testing (INASMET) of TStE355 steel samples in contact with saturated bentonite at temperatures of up to 100°C , for which generalised corrosion rates of up to 10 microns/year were measured. However, the Cu-ETP test pieces underwent similar generalised corrosion rates, $0.71 \mu\text{m}/\text{year}$, as those measured in the bentonite tests referred to above, with a measured corrosion rate of $0.5 \mu\text{m}/\text{year}$. The Cu-30Ni alloy underwent a similar degree of corrosion to that observed in said experiments.

The slight corrosion suffered by the steel can be attributed to the low humidity content of the bentonite housing the samples, very far from saturation level (25.5%), as well as to the almost anoxic conditions within the “in situ” test. With the copper, as well as the oxygen that forms cuprite, which is a passive, protective oxide, the presence of chlorine—as chloride—generates non-protective species, such as the CuCl_2 , detected in one of the XRD analyses carried

out. The bentonite analysed gives a significant concentration of chlorides, which would justify the corrosion rate values obtained with the copper test pieces.

Finally, and given that the carbon steel and copper racks were tested in different blocks of bentonite, it should not be assumed that the humidity conditions were the same during the tests. In this sense, we should point out that the block the copper test pieces were in, showed a slightly higher humidity loss (13.4%), to that shown by the bentonite block with the carbon steel coupons (13.1%).

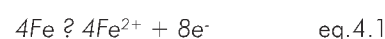
Sensors

The four sensors studied were by far the components with the greatest corrosion damage.

The most significant feature shown by analysis of the corrosion products generated is a significant presence of sulphur. Microbiological analysis of the bentonite enveloping the sensor reveals a significant presence of sulphate reducing bacteria (SRB) content that increases, when the remains of bentonite and corrosion products, still adhered to the sensors in the form of pustules, are analysed. This leads us to establish the main cause of the corrosion damage observed, a local corrosion phenomena induced by the presence of SRB in the bentonite, as well as the higher humidity content of the bentonite the further we move away radially from the heater. As a consequence of the metabolic activity of SRB, sulphides are generated and thus a very corrosive environment, which in this case is responsible for the significant corrosion damage observed. In this case, the source of the sulphates is the bentonite itself.

The mechanism proposed to explain the corrosion of the steel by SRB bacteria is as follows:

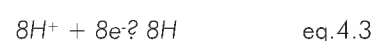
- Anodic reaction



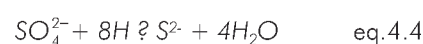
- Water dissociation



- Cathodic reaction



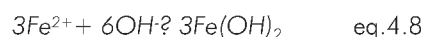
- Cathodic depolarisation by bacteria (BSR)



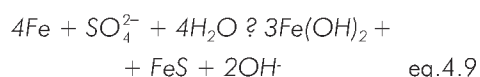
□ Corrosion products



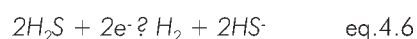
□ Corrosion products



Combining all the above equations, we reach the following overall reaction:



There are two more reactions that can occur throughout the process and which generate H_2S and HS^- as intermediate species, which are very corrosive to metals:



The SRB are exclusively anaerobic bacteria, meaning that they only grow in the absence of oxygen. However, in aerobic conditions they can develop under other bacterial colonies or deposits, beneath which a zone lacking or deficient in oxygen is created. These would explain why, as well as aerobic bacteria, groups of anaerobic bacteria like the sulphate reducers were detected in the samples of bentonite with biological activity. At the beginning, the aerobic bacteria groups can grow on the surface of the metal, allowing the SRB to grow in anaerobic conditions within the biofilm.

As well as localised corrosion by pitting, transgranular cracking was observed on sensor SH-SD1-02 and on a rock fixing plate. The ramified morphology of the cracks is typical of Stress Corrosion Cracking (SCC) in stainless steels. This localised corrosion phenomena develops with the simultaneous action of a stress, residual or applied, and a corrosive agent, normally chlorides in the case of stainless steels. Sometimes the stress corrosion cracking starts from the pitting, which act as stress concentration centres. We cannot rule out that the presence of other depassivating corrosion agents (as well as the chlorides) resulting from the metabolic activity of the SRB such as S^{2-} and/or HS^- has contributed to the stress corrosion cracking observed. In this sense, SCC is quite frequently observed in association with corrosion phenomena induced by bacteria.

With microbiological corrosion of steels, the corrosion products generated are normally black iron sulphides. Most of the sulphides generated are amor-

phous and not crystalline, meaning that the XRD results should be treated with caution. This would explain why only Pyrrhotite with the molecular formula Fe_{1-x}S is detected in the XRD spectrum of green corrosion products observed on the sensors. EDS analysis of the bentonite surrounding the test pieces reveals chrome enrichment. Thus, we do not discard the possibility of the green corrosion products observed corresponding to green, amorphous hydrated chrome oxides of type $\text{Cr}_2\text{O}_3 \cdot \text{H}_2\text{O}$.

EDS analysis of the pustules, with their characteristic dark brown deposits, identifies significant amounts of calcium, sulphur and iron. The XRD spectrum only detects calcite, CaCO_3 , given the amorphous nature of the iron sulphides. The formation of crystallised calcite (Figure 104) is usually attributed to chemical transformations of the deposits or pustules, which are usually accompanied by the precipitation of calcite. These deposits normally reflect SRB corrosion that is no longer active.

With the thermocouples, as well as green and black corrosion products, yellow corrosion products rich in chlorine and nickel are also generated. This could indicate the formation of nickel chlorides (yellow) with the molecular formula NiCl_2 . Therefore, as well as corrosion induced by bacteria, there is corrosion or dissolution of the metal due to the effect of the chlorides in the environment.

To summarise, we can conclude that the significant corrosion damage suffered by these components is due to the following two main causes:

- the presence of sulphate reducing bacteria, and
- the high humidity of the bentonite blocks housing them

Bentonite

The results obtained from microbiological characterisation of the bentonite samples show significant bacterial activity, with a major population of SRB in the block of bentonite housing one of the sensors. The opposite is true of the block of bentonite identified as BS24-3, located very close to the heater, which shows a total absence of aerobic, anaerobic and sulphate reducing bacteria (SRB). The absence of biological activity is basically attributed to the high temperature reached by this block during the test. Here we should point out that most bacteria and microorganisms usually involved in microbiological corrosion phenomena have a "survival" ran-

ge of between 10 and 50°C, as is the case with the SRB. The absence of humidity inhibits the growth of the bacteria, slowing down their activity, but does not eliminate them.

After analysing the results we obtain in [Figure 133](#) to explain the evolution of the corrosion suffered by the different components, in function of the temperature and humidity of the “in situ” test.

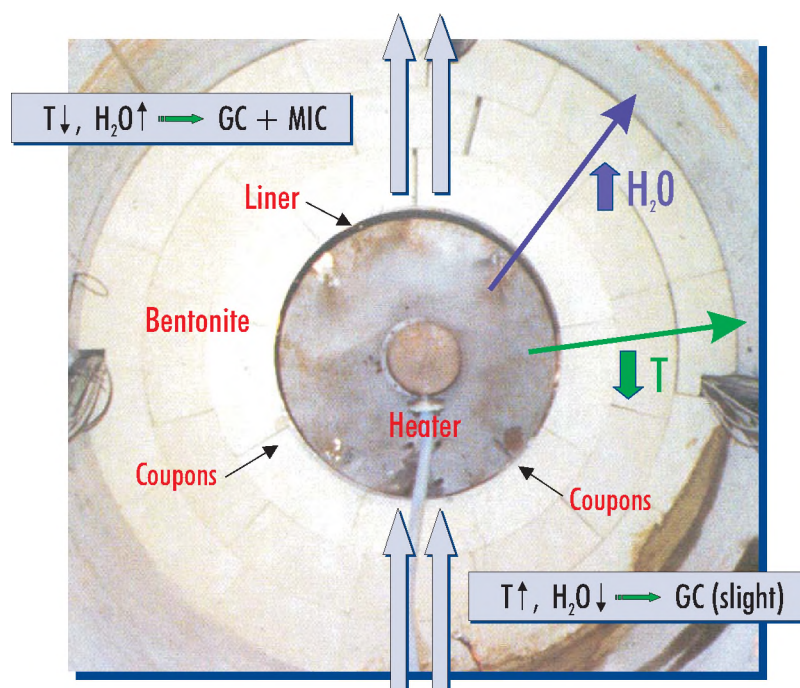


Figure 133. Evolution of the corrosion suffered by the different components, in function of the temperature and humidity of the “in situ” test. GC: Generalised Corrosion. MIC: Microbiologically Induced Corrosion



5. Conclusions



5. Conclusions

The following conclusions can be reached on the basis of the results obtained:

Heater

- ❑ It shows slight uniform generalised corrosion over its whole surface, with oxide layers less than 20 microns thick in all the cases examined.
- ❑ No localised corrosion phenomena were observed.

Liner

- ❑ The morphology of the corrosion detected on the liner was generalised and non-uniform, with maximum values of penetration of the corrosion of approximately 130 microns on the external surface and 200 microns on the internal surface.
- ❑ No localised corrosion phenomena were observed.

Corrosion Coupons

- ❑ No generalised and/or local corrosion was observed on the stainless steel and titanium specimens.

- ❑ The carbon steel coupons showed very slight generalised corrosion, with corrosion rate values of $0.10 \mu\text{m}/\text{year}$. No localised corrosion phenomena were detected.
- ❑ The copper coupons showed corrosion rates of $0.71 \mu\text{m}/\text{year}$ for the Cu-ETP, and $0.74 \mu\text{m}/\text{year}$ for the Cu10Ni alloy. The corrosion suffered by the Cu30Ni alloy was negligible.

Sensors

- ❑ The high humidity, together with the presence of sulphate reducing bacteria in the bentonite housing the sensors are the reasons behind the significant corrosion observed in these components. The sulphur rich corrosion products, as well as the morphology of the corrosion indicate a localised corrosion phenomena induced by sulphate reducing bacteria.
- ❑ Cracking typical of stress corrosion induced by the presence of chlorides and/or products resulting from the metabolic activity of the SRB was also observed.
- ❑ With the carbon steel components, the corrosion observed was of the generalised type, with the practical destruction of the component being observed on occasions.



6. Annex



6. Annex

FEBEX Project Components: Corrosion Study

INASMET: Characterization Department	Ref. 36.0045.0	03 June 2003
--------------------------------------	----------------	--------------

CERTIFICATE OF MICROHARDNESS

Sample reference	Heater (c)		
Test:	HV 10		
Standard / Procedure	ISO 6507.1		
Equipment: 61.085.01	Standard ref.: 61.921.11	Temperature: 22 ± 2°C	

TRACE LOCALIZATION



RESULTS

1	2	3	4	5	6	7	8	9	10	11	12
158	159	229	220	227	225	228	230	201	190	142	145

OBSERVATION (*) Details supplied by the client

Tester / analyst: M. Berasarte	Head of Metallography: F. Marin
Carried out: Date of Test: 12/09/02	Carried out: Date of Test: 12/09/02

FEBEX Project Components: Corrosion Study

INASMET: Characterization Department Ref. 36.0045.0 03 June 2003

CERTIFICADO DE ANALISIS - CERTIFICAT D'ANALYSE
CERTIFICATE OF ANALYSIS - ANALITICALERZEUGNIS

Client: R 442

Reference (*): Plate fixing to rock SH-SD1-01

ELEMENTS ANALYSED
Values expressed as (%)

SAMPLE	C	Si	Mn	P	S	Cr	Ni	Mo
*	0.050	0.40	1.3	0.026	<0.005	18.3	8.7	0.25
	Cu							
	0.20							

Stainless steels: Analytical Methodology			Standard reference	
	Procedure		Low and medium alloy steels	Stainless steels
<input checked="" type="checkbox"/> C y S	Automatic Analyser	31-O-002	<input type="checkbox"/> NIST C1221	<input type="checkbox"/> BAS/SS 461
<input type="checkbox"/> N	Automatic Analyser	31-O-003	<input type="checkbox"/> NIST 1264a	<input type="checkbox"/> BAS/SS 462
<input type="checkbox"/> O	Automatic Analyser	31-O-003	<input type="checkbox"/> BAS/SS 406/1	<input type="checkbox"/> BAS/SS 463
<input type="checkbox"/> C	Emission Spectrometry - Spark	31-O-050	<input type="checkbox"/> BAS/SS 407/1	<input type="checkbox"/> BAS/SS 464/1
<input type="checkbox"/> S	Emission Spectrometry - Spark	31-O-050	<input type="checkbox"/> BAS/SS 408/1	<input checked="" type="checkbox"/> BAS/SS 465
<input checked="" type="checkbox"/> Si	Emission Spectrometry - Spark	31-O-050	<input type="checkbox"/> BAS/SS 409/1	<input checked="" type="checkbox"/> BAS/SS 466/1
<input checked="" type="checkbox"/> Mn	Emission Spectrometry - Spark	31-O-050	<input type="checkbox"/> BAS/SS 410/1	<input type="checkbox"/> BAS/SS 467/1
<input checked="" type="checkbox"/> P	Emission Spectrometry - Spark	31-O-050	<input type="checkbox"/> BCS 456	<input type="checkbox"/> BAS/SS 468
<input checked="" type="checkbox"/> Cr	Emission Spectrometry - Spark	31-O-050	<input type="checkbox"/> BCS 460	<input type="checkbox"/> BCS/SS-CRM 474
<input checked="" type="checkbox"/> Ni	Emission Spectrometry - Spark	31-O-050	<input type="checkbox"/> CV-7	<input checked="" type="checkbox"/> BCS/SS-CRM 475
<input checked="" type="checkbox"/> Mo	Emission Spectrometry - Spark	31-O-050	<input type="checkbox"/> CV-22	<input type="checkbox"/> BCS/SS-CRM 464/1
<input type="checkbox"/> V	Emission Spectrometry - Spark	31-O-050	<input type="checkbox"/> CV-31	<input type="checkbox"/> BCS/SS-CRM 465/1
<input type="checkbox"/> Ti	Emission Spectrometry - Spark	31-O-050	<input type="checkbox"/> ECRM 077-2	<input type="checkbox"/> BCS/SS 261/1
<input type="checkbox"/> Mg	Emission Spectrometry - Spark	31-O-050	<input type="checkbox"/> ECRM 082-1	<input checked="" type="checkbox"/> Euronorm-ZRM-237-1
<input type="checkbox"/> Al	Emission Spectrometry - Spark	31-O-050	<input type="checkbox"/> Euro ZRM 184-1	<input type="checkbox"/> Euronorm-MRC 282-1
<input type="checkbox"/> Nb	Emission Spectrometry - Spark	31-O-050	<input type="checkbox"/> Euronorm-CRM 087-1	<input type="checkbox"/> ECRM 281-1
<input checked="" type="checkbox"/> Cu	Emission Spectrometry - Spark	31-O-050	<input type="checkbox"/> Euronorm-CRM 186-1	<input type="checkbox"/> CRM JK 27A
			<input type="checkbox"/> BCS 225/2	<input type="checkbox"/> BCS 339
			<input type="checkbox"/> BCS 306/1	<input type="checkbox"/> BCS 342
			<input type="checkbox"/> BCS/SS-CRM 402/2	<input type="checkbox"/> LECO 501-502
			<input type="checkbox"/> BCS-CRM 458/1	
			<input type="checkbox"/> LECO 501-503	
Comments: (*) data supplied by client			Test Date: 25-09-02	
			INASMET Carried out by: Karmele Izquierdo Head of Chemical Characterisation	

* Este certificado carece de valor fuera del contexto del informe al que pertenece
This certificate has no value outside the context of the report it refers to.

* Este certificado carece de valor fuera del contexto del informe al que pertenece

FEBEX Project Components: Corrosion Study

INASMET: Characterization Department Ref. 36.0045.0 03 June 2003

CERTIFICADO DE ANALISIS - CERTIFICAT D'ANALYSE
CERTIFICATE OF ANALYSIS - A NALITICALERZEUGNIS

Client: R 442

Reference (*): Sensor Tube SH-SD1-01

ELEMENTS ANALYSED
Values expressed as (%)

SAMPLE	C	Si	Mn	P	S	Cr	Ni	Mo
*	0.024	0.44	1.6	0.028	0.005	17.1	12.3	2.0

Stainless Steels: Analytical Methodology**Procedure****Standard reference**

- ☒ C Automatic Analyser
- ☒ S Automatic Analyser
- ☐ O Automatic Analyser
- ☐ N Automatic Analyser
- ☐ Si Gravimetric method
- ☒ Si Emission Spectrometry (ICP-AES)
- ☒ Mn Emission Spectrometry (ICP-AES)
- ☒ P Emission Spectrometry (ICP-AES)
- ☒ Cr Volumetric method
- ☒ Ni Gravimetric method
- ☐ Ni Emission Spectrometry (ICP-AES)
- ☒ Mo Emission Spectrometry (ICP-AES)
- ☐ Ti Emission Spectrometry (ICP-AES)
- ☐ Nb Emission Spectrometry (ICP-AES)
- ☐ V Emission Spectrometry (ICP-AES)
- ☐ Al Emission Spectrometry (ICP-AES)
- ☐ Cu Emission Spectrometry (ICP-AES)

- 31-O-002
- 31-O-002
- 31-O-003
- 31-O-003
- 31-O-004
- 31-O-008
- 31-O-008
- 31-O-008
- 31-O-007
- 31-O-006
- 31-O-008
- 31-O-008
- 31-O-008
- 31-O-008
- 31-O-008
- 31-O-008
- 31-O-008

- ☐ BCS/SS-CRM 464/1
- ☐ BCS/SS-CRM 465/1
- ☐ BCS/SS-CRM 466/1
- ☒ BCS/SS-CRM 474
- ☐ BCS/SS 261/1
- ☐ BCS/SS 494
- ☐ BCS 338
- ☐ BCS 339
- ☐ BCS 342
- ☒ CRM JK 27A
- ☐ ECRM 281-1
- ☒ Euronorm-ZRM 237-1
- ☒ Euronorm-MRC 282-1
- ☐ LECO 501-147
- ☐ LECO 501-148
- ☒ LECO 501-503
- ☐ LECO 501-550
- ☐ LECO 501-644
- ☐ LECO 501-645
- ☐ LECO 501-647
- ☐ LECO 502-016
- ☐ LECO 501-643
- ☐ LECO 502-256

Comments: (*) data supplied by client**Test Date: 27-09-02****INASMET**

The uncertainty associated with measurement of the results expressed in this certificate is at the disposition of the client.

Carried out by: Karmele Izquierdo
Head of Chemical
Characterisation

Procedure 31-G-001

This certificate has no value outside the context of the report it refers to.

PUBLICACIONES TÉCNICAS

1991

- 01 REVISIÓN SOBRE LOS MODELOS NUMÉRICOS RELACIONADOS CON EL ALMACENAMIENTO DE RESIDUOS RADIACTIVOS.
- 02 REVISIÓN SOBRE LOS MODELOS NUMÉRICOS RELACIONADO CON EL ALMACENAMIENTO DE RESIDUOS RADIACTIVOS. ANEXO 1. *Guía de códigos aplicables.*
- 03 PRELIMINARY SOLUBILITY STUDIES OF URANIUM DIOXIDE UNDER THE CONDITIONS EXPECTED IN A SALINE REPOSITORY.
- 04 GEOESTADÍSTICA PARA EL ANÁLISIS DE RIESGOS. *Una introducción a la Geostatística no paramétrica.*
- 05 SITUACIONES SINÓPTICAS Y CAMPOS DE VIENTOS ASOCIADOS EN "EL CABRIL".
- 06 PARAMETERS, METHODOLOGIES AND PRIORITIES OF SITE SELECTION FOR RADIOACTIVE WASTE DISPOSAL IN ROCK SALT FORMATIONS.

1992

- 01 STATE OF THE ART REPORT: DISPOSAL OF RADIOACTIVE WASTE IN DEEP ARGILLACEOUS FORMATIONS.
- 02 ESTUDIO DE LA INFILTRACIÓN A TRAVÉS DE LA COBERTERA DE LA FUA.
- 03 SPANISH PARTICIPATION IN THE INTERNATIONAL INTRAVAL PROJECT.
- 04 CARACTERIZACIÓN DE ESMECTITAS MAGNÉSICAS DE LA CUENCA DE MADRID COMO MATERIALES DE SELLADO. *Ensayos de alteración hidrotermal.*
- 05 SOLUBILITY STUDIES OF URANIUM DIOXIDE UNDER THE CONDITIONS EXPECTED IN A SALINE REPOSITORY. *Phase II*
- 06 REVISIÓN DE MÉTODOS GEOFÍSICOS APPLICABLES AL ESTUDIO Y CARACTERIZACIÓN DE EMPLAZAMIENTOS PARA ALMACENAMIENTO DE RESIDUOS RADIACTIVOS DE ALTA ACTIVIDAD EN GRANITOS, SALES Y ARCILLAS.
- 07 COEFICIENTES DE DISTRIBUCIÓN ENTRE RADIONUCLEIDOS.
- 08 CONTRIBUTION BY CTN-UPM TO THE PSACON LEVELS EXERCISE.
- 09 DESARROLLO DE UN MODELO DE RESUSPENSIÓN DE SUELOS CONTAMINADOS. APLICACIÓN AL ÁREA DE PALOMARES.
- 10 ESTUDIO DEL CÓDIGO FFSM PARA CAMPO LEJANO. *IMPLANTACIÓN EN VAX.*
- 11 LA EVALUACIÓN DE LA SEGURIDAD DE LOS SISTEMAS DE ALMACENAMIENTO DE RESIDUOS RADIACTIVOS. UTILIZACIÓN DE MÉTODOS PROBABILISTAS.
- 12 METODOLOGÍA CANADIENSE DE EVALUACIÓN DE LA SEGURIDAD DE LOS ALMACENAMIENTOS DE RESIDUOS RADIACTIVOS.
- 13 DESCRIPCIÓN DE LA BASE DE DATOS WALKER.

Publicaciones no periódicas

PONENCIAS E INFORMES, 1988-1991.
SEGUNDO PLAN DE I+D, 1991-1995. TOMOS I, II Y III.
SECOND RESEARCH AND DEVELOPMENT PLAN, 1991-1995, VOLUME I.

1993

- 01 INVESTIGACIÓN DE BENTONITAS COMO MATERIALES DE SELLADO PARA ALMACENAMIENTO DE RESIDUOS RADIACTIVOS DE ALTA ACTIVIDAD. ZONA DE CABO DE GATA, ALMERÍA.
- 02 TEMPERATURA DISTRIBUTION IN A HYPOTHETICAL SPENT NUCLEAR FUEL REPOSITORY IN A SALT DOME.
- 03 ANÁLISIS DEL CONTENIDO EN AGUA EN FORMACIONES SALINAS. *Su aplicación al almacenamiento de residuos radiactivos*
- 04 SPANISH PARTICIPATION IN THE HAW PROJECT. *Laboratory Investigations on Gamma Irradiation Effects in Rock Salt.*
- 05 CARACTERIZACIÓN Y VALIDACIÓN INDUSTRIAL DE MATERIALES ARCILLOSOS COMO BARRERA DE INGENIERÍA.
- 06 CHEMISTRY OF URANIUM IN BRINES RELATED TO THE SPENT FUEL DISPOSAL IN A SALT REPOSITORY (I).
- 07 SIMULACIÓN TÉRMICA DEL ALMACENAMIENTO EN GALERÍA-TSS.
- 08 PROGRAMAS COMPLEMENTARIOS PARA EL ANÁLISIS ESTOCASTICO DEL TRANSPORTE DE RADIONUCLEIDOS.
- 09 PROGRAMAS PARA EL CÁLCULO DE PERMEABILIDADES DE BLOQUE.
- 10 METHODS AND RESULTS OF THE INVESTIGATION OF THE THERMOMECHANICAL BEHAVIOUR OF ROCK SALT WITH REGARD TO THE FINAL DISPOSAL OF HIGH-LEVEL RADIOACTIVE WASTES.

Publicaciones no periódicas

SEGUNDO PLAN DE I+D. INFORME ANUAL 1992.
PRIMERAS JORNADAS DE I+D EN LA GESTIÓN DE RESIDUOS RADIACTIVOS. TOMOS I Y II.

1994

- 01 MODELO CONCEPTUAL DE FUNCIONAMIENTO DE LOS ECOSISTEMAS EN EL ENTORNO DE LA FÁBRICA DE URANIO DE ANDÚJAR.
- 02 CORROSION OF CANDIDATE MATERIALS FOR CANISTER APPLICATIONS IN ROCK SALT FORMATIONS.
- 03 STOCHASTIC MODELING OF GROUNDWATER TRAVEL TIMES
- 04 THE DISPOSAL OF HIGH LEVEL RADIOACTIVE WASTE IN ARGILLACEOUS HOST ROCKS. *Identification of parameters, constraints and geological assessment priorities.*
- 05 EL DESTE DE EUROPA Y LA PENÍNSULA IBÉRICA DESDE HACE 120.000 AÑOS HASTA EL PRESENTE. *Isostasia glacial, paleogeografía paleotemperaturas.*
- 06 ECOLOGÍA EN LOS SISTEMAS ACUÁTICOS EN EL ENTORNO DE EL CABRIL.
- 07 ALMACENAMIENTO GEOLÓGICO PROFUNDO DE RESIDUOS RADIACTIVOS DE ALTA ACTIVIDAD (AGP). *Conceptos preliminares de referencia.*
- 08 UNIDADES MÓVILES PARA CARACTERIZACIÓN HIDROGEOQUÍMICA
- 09 EXPERIENCIAS PRELIMINARES DE MIGRACIÓN DE RADIONUCLEIDOS CON MATERIALES GRANÍTICOS. EL BERROCAL, ESPAÑA.
- 10 ESTUDIOS DE DESEQUILIBRIOS ISOTÓPICOS DE SERIES RADIACTIVAS NATURALES EN UN AMBIENTE GRANÍTICO: PLUTÓN DE EL BERROCAL (TOLEDO).
- 11 RELACIÓN ENTRE PARÁMETROS GEOFÍSICOS E HIDROGEOLÓGICOS. *Una revisión de literatura.*
- 12 DISEÑO Y CONSTRUCCIÓN DE LA COBERTURA MULTICAPA DEL DIQUE DE ESTÉRILES DE LA FÁBRICA DE URANIO DE ANDÚJAR.

Publicaciones no periódicas

SEGUNDO PLAN I+D 1991-1995. INFORME ANUAL 1993.

1995

- 01 DETERMINACIÓN DEL MÓDULO DE ELASTICIDAD DE FORMACIONES ARCILLOSAS PROFUNDAS.
- 02 UO LEACHING AND RADIONUCLIDE RELEASE MODELLING UNDER HIGH AND LOW IONIC STRENGTH SOLUTION AND OXIDATION CONDITIONS.
- 03 THERMO-HYDRO-MECHANICAL CHARACTERIZATION OF THE SPANISH REFERENCE CLAY MATERIAL FOR ENGINEERED BARRIER FOR GRANITE AND CLAY HLW REPOSITORY: LABORATORY AND SMALL MOCK UP TESTING.
- 04 DOCUMENTO DE SÍNTESIS DE LA ASISTENCIA GEOTÉCNICA AL DISEÑO AGPARCILLA. *Concepto de referencia.*
- 05 DETERMINACIÓN DE LA ENERGÍA ACUMULADA EN LAS ROCAS SALINAS FUERTEMENTE IRRADIADAS MEDIANTE TÉCNICAS DE TERMOLUMINISCENCIA. *Aplicación al análisis de repositorios de residuos radiactivos de alta actividad.*
- 06 PREDICCIÓN DE FENÓMENOS DE TRANSPORTE EN CAMPO PRÓXIMO Y LEJANO. *Interacción en fases sólidas.*
- 07 ASPECTOS RELACIONADOS CON LA PROTECCIÓN RADIOLÓGICA DURANTE EL DESMANTELAMIENTO Y CLAUSURA DE LA FÁBRICA DE ANDÚJAR.
- 08 ANALYSIS OF GAS GENERATION MECHANISMS IN UNDERGROUND RADIOACTIVE WASTE REPOSITORIES. *(Pegase Project).*
- 09 ENSAYOS DE LIXIVIACIÓN DE EMISORES BETA PUROS DE LARGA VIDA.
- 10 2º PLAN DE I+D. DESARROLLOS METODOLÓGICOS, TECNOLÓGICOS, INSTRUMENTALES Y NUMÉRICOS EN LA GESTIÓN DE RESIDUOS RADIACTIVOS.
- 11 PROYECTO AGP-ALMACENAMIENTO GEOLÓGICO PROFUNDO. FASE 2.
- 12 IN SITU INVESTIGATION OF THE LONG-TERM SEALING SYSTEM AS COMPONENT OF DAM CONSTRUCTION (DAM PROJECT). *Numerical simulator: Code-Bright.*

Publicaciones no periódicas

TERCER PLAN DE I+D 1995-1999.
SEGUNDAS JORNADAS DE I+D. EN LA GESTIÓN DE RESIDUOS RADIACTIVOS. TOMOS I Y II.

1996

- 01 DESARROLLO DE UN PROGRAMA INFORMÁTICO PARA EL ASESORAMIENTO DE LA OPERACIÓN DE FOCOS EMISORES DE CONTAMINANTES GASEOSOS.
- 02 FINAL REPORT OF PHYSICAL TEST PROGRAM CONCERNING SPANISH CLAYS (SAPONITES AND BENTONITES).
- 03 APORTACIONES AL CONOCIMIENTO DE LA EVOLUCIÓN PALEOCLIMÁTICA Y PALEOAMBIENTAL EN LA PENÍNSULA IBÉRICA DURANTE LOS DOS ÚLTIMOS MILLONES DE AÑOS A PARTIR DEL ESTUDIO DE TRAVERTINOS Y ESPELEOTEMAS.
- 04 MÉTODOS GEOESTADÍSTICOS PARA LA INTEGRACIÓN DE INFORMACIÓN.
- 05 ESTUDIO DE LONGEVIDAD EN BENTONITAS: ESTABILIDAD HIDROTÉRMICA DE SAPONITAS.
- 06 ALTERACIÓN HIDROTÉRMICA DE LAS BENTONITAS DE ALMERÍA.
- 07 MAYDAY. UN CÓDIGO PARA REALIZAR ANÁLISIS DE INCERTIDUMBRE Y SENSIBILIDAD. *Manuales.*

Publicaciones no periódicas

EL BERROCAL PROJECT. VOLUME I. GEOLOGICAL STUDIES.
EL BERROCAL PROJECT. VOLUME II. HYDROGEOCHEMISTRY.
EL BERROCAL PROJECT. VOLUME III. LABORATORY MIGRATION TESTS AND IN SITU TRACER TEST.
EL BERROCAL PROJECT. VOLUME IV. HYDROGEOLOGICAL MODELLING AND CODE DEVELOPMENT.

1997

- 01 CONSIDERACIÓN DEL CAMBIO MEDIOAMBIENTAL EN LA EVALUACIÓN DE LA SEGURIDAD. ESCENARIOS CLIMÁTICOS A LARGO PLAZO EN LA PENÍNSULA IBÉRICA.
- 02 METODOLOGÍA DE EVALUACIÓN DE RIESGO SÍSMICO EN SEGMENTOS DE FALLA.
- 03 DETERMINACIÓN DE RADIONUCLEIDOS PRESENTES EN EL INVENTARIO DE REFERENCIA DEL CENTRO DE ALMACENAMIENTO DE EL CABRIL.
- 04 ALMACENAMIENTO DEFINITIVO DE RESIDUOS DE RADIACTIVIDAD ALTA. *Caracterización y comportamiento a largo plazo de los combustibles nucleares irradiados (I).*
- 05 METODOLOGÍA DE ANÁLISIS DE LA BIOSFERA EN LA EVALUACIÓN DE ALMACENAMIENTOS GEOLÓGICOS PROFUNDOS DE RESIDUOS RADIACTIVOS DE ALTA ACTIVIDAD ESPECÍFICA.
- 06 EVALUACIÓN DEL COMPORTAMIENTO Y DE LA SEGURIDAD DE UN ALMACENAMIENTO GEOLÓGICO PROFUNDO EN GRANITO. *Marzo 1997*
- 07 SÍNTESIS TECTOESTRATIGRÁFICA DEL MACIZO HESPÉRCICO. VOLUMEN I.
- 08 III JORNADAS DE I+D Y TECNOLOGÍAS DE GESTIÓN DE RESIDUOS RADIACTIVOS. *Posters descriptivos de los proyectos de I+D y evaluación de la seguridad a largo plazo.*
- 09 FEBEX. ETAPA PREOPERACIONAL. INFORME DE SÍNTESIS.
- 10 METODOLOGÍA DE GENERACIÓN DE ESCENARIOS PARA LA EVALUACIÓN DEL COMPORTAMIENTO DE LOS ALMACENAMIENTOS DE RESIDUOS RADIACTIVOS.
- 11 MANUAL DE CESARR V.2. *Código para la evaluación de seguridad de un almacenamiento superficial de residuos radiactivos de baja y media actividad.*

1998

- 01 FEBEX. PRE-OPERATIONAL STAGE. SUMMARY REPORT.
- 02 PERFORMANCE ASSESSMENT OF A DEEP GEOLOGICAL REPOSITORY IN GRANITE. *March 1997.*
- 03 FEBEX. DISEÑO FINAL Y MONTAJE DEL ENSAYO "IN SITU" EN GRIMSEL.
- 04 FEBEX. BENTONITA: ORIGEN, PROPIEDADES Y FABRICACIÓN DE BLOQUES.
- 05 FEBEX. BENTONITE: ORIGIN, PROPERTIES AND FABRICATION OF BLOCKS.
- 06 TERCERAS JORNADAS DE I+D Y TECNOLOGÍAS DE GESTIÓN DE RESIDUOS RADIACTIVOS. 24-29 Noviembre, 1997. *Volumen I*
- 07 TERCERAS JORNADAS DE I+D Y TECNOLOGÍAS DE GESTIÓN DE RESIDUOS RADIACTIVOS. 24-29 Noviembre, 1997. *Volumen II*
- 08 MODELIZACIÓN Y SIMULACIÓN DE BARRERAS CAPILARES.
- 09 FEBEX. PREOPERATIONAL THERMO-HYDRO-MECHANICAL (THM) MODELLING OF THE "IN SITU" TEST.

Títulos publicados

- 10 FEBEX. PREOPERATIONAL THERMO-HYDRO-MECHANICAL (THM) MODELLING OF THE "MOCK UP" TEST.
- 11 DISOLUCIÓN DEL UO₂(s) EN CONDICIONES REDUCTORAS Y OXIDANTES.
- 12 FEBEX. FINAL DESIGN AND INSTALLATION OF THE "IN SITU" TEST AT GRIMSEL.

1999

- 01 MATERIALES ALTERNATIVOS DE LA CÁPSULA DE ALMACENAMIENTO DE RESIDUOS RADIACTIVOS DE ALTA ACTIVIDAD.
- 02 INTRAVAL PROJECT PHASE 2: STOCHASTIC ANALYSIS OF RADIONUCLIDES TRAVEL TIMES AT THE WASTE ISOLATION PILOT PLANT (WIPP), IN NEW MEXICO (U.S.A.).
- 03 EVALUACIÓN DEL COMPORTAMIENTO Y DE LA SEGURIDAD DE UN ALMACENAMIENTO PROFUNDO EN ARCILLA. Febrero 1999.
- 04 ESTUDIOS DE CORROSIÓN DE MATERIALES METÁLICOS PARA CÁPSULAS DE ALMACENAMIENTO DE RESIDUOS DE ALTA ACTIVIDAD.
- 05 MANUAL DEL USUARIO DEL PROGRAMA VISUAL BALAN V. 1.0. CÓDIGO INTERACTIVO PARA LA REALIZACIÓN DE BALANCES HIDROLÓGICOS Y LA ESTIMACIÓN DE LA RECARGA.
- 06 COMPORTAMIENTO FÍSICO DE LAS CÁPSULAS DE ALMACENAMIENTO.
- 07 PARTICIPACIÓN DEL CIEMAT EN ESTUDIOS DE RADIOECOLOGÍA EN ECOSISTEMAS MARINOS EUROPEOS.
- 08 PLAN DE INVESTIGACIÓN Y DESARROLLO TECNOLÓGICO PARA LA GESTIÓN DE RESIDUOS RADIACTIVOS 1999-2003. OCTUBRE 1999.
- 09 ESTRATIGRAFÍA BIOMOLECULAR. LA RACEMIZACIÓN/EPIMERIZACIÓN DE AMINOÁCIDOS COMO HERRAMIENTA GEOCRONOLÓGICA Y PALEOTERMOMÉTRICA.
- 10 CATSIUS CLAY PROJECT. Calculation and testing of behaviour of unsaturated clay as barrier in radioactive waste repositories. STAGE 1: VERIFICATION EXERCISES.
- 11 CATSIUS CLAY PROJECT. Calculation and testing of behaviour of unsaturated clay as barrier in radioactive waste repositories. STAGE 2: VALIDATION EXERCISES AT LABORATORY SCALE.
- 12 CATSIUS CLAY PROJECT. Calculation and testing of behaviour of unsaturated clay as barrier in radioactive waste repositories. STAGE 3: VALIDATION EXERCISES AT LARGE "IN SITU" SCALE.

2000

- 01 FEBEX PROJECT. FULL-SCALE ENGINEERED BARRIERS EXPERIMENT FOR A DEEP GEOLOGICAL REPOSITORY FOR HIGH LEVEL RADIOACTIVE WASTE IN CRYSTALLINE HOST ROCK. FINAL REPORT.
- 02 CÁLCULO DE LA GENERACIÓN DE PRODUCTOS RADIOLÍTICOS EN AGUA POR RADIACIÓN α . DETERMINACIÓN DE LA VELOCIDAD DE ALTERACIÓN DE LA MATRIZ DEL COMBUSTIBLE NUCLEAR GASTADO.
- 03 LIBERACIÓN DE RADIONUCLEÍDOS E ISÓTOPOS ESTABLES CONTENIDOS EN LA MATRIZ DEL COMBUSTIBLE. MODELO CONCEPTUAL Y MODELO MATEMÁTICO DEL COMPORTAMIENTO DEL RESIDUO.
- 04 DESARROLLO DE UN MODELO GEOQUÍMICO DE CAMPO PRÓXIMO.
- 05 ESTUDIOS DE DISOLUCIÓN DE ANÁLOGOS NATURALES DE COMBUSTIBLE NUCLEAR IRRADIADO Y DE FASES DE (U)VI-SILICIO REPRESENTATIVAS DE UN PROCESO DE ALTERACIÓN OXIDATIVA.
- 06 CORE2D. A CODE FOR NON-ISOTHERMAL WATER FLOW AND REACTIVE SOLUTE TRANSPORT. USERS MANUAL VERSION 2.
- 07 ANÁLOGOS ARQUEOLÓGICOS E INDUSTRIALES PARA ALMACENAMIENTOS PROFUNDOS. ESTUDIO DE PIEZAS ARQUEOLÓGICAS METÁLICAS.

- 08 PLAN DE INVESTIGACIÓN Y DESARROLLO TECNOLÓGICO PARA LA GESTIÓN DE RESIDUOS RADIACTIVOS 1999-2003. REVISIÓN 2000.
- 09 IV JORNADAS DE INVESTIGACIÓN Y DESARROLLO TECNOLÓGICO EN GESTIÓN DE RESIDUOS RADIACTIVOS. POSTERS DIVULGATIVOS.
- 10 IV JORNADAS DE INVESTIGACIÓN Y DESARROLLO TECNOLÓGICO EN GESTIÓN DE RESIDUOS RADIACTIVOS. POSTERS TÉCNICOS.
- 11 PROGRAMA DE INVESTIGACIÓN PARA ESTUDIAR LOS EFECTOS DE LA RADIACIÓN GAMMA EN BENTONITAS CÁLCICAS ESPAÑOLAS.
- 12 CARACTERIZACIÓN Y LIXIVIACIÓN DE COMBUSTIBLES NUCLEARES IRRADIADOS Y DE SUS ANÁLOGOS QUÍMICOS.

2001

- 01 MODELOS DE FLUJO MULTIFÁSICO NO ISOTERMO Y DE TRANSPORTE REACTIVO MULTICOMPONENTE EN MEDIOS POROSOS.
- 02 IV JORNADAS DE INVESTIGACIÓN Y DESARROLLO TECNOLÓGICO EN GESTIÓN DE RESIDUOS RADIACTIVOS. RESÚMENES Y ABSTRACTS.
- 03 ALMACENAMIENTO DEFINITIVO DE RESIDUOS DE RADIACTIVIDAD ALTA. CARACTERIZACIÓN Y COMPORTAMIENTO A LARGO PLAZO DE LOS COMBUSTIBLES NUCLEARES IRRADIADOS (II).
- 04 CONSIDERATIONS ON POSSIBLE SPENT FUEL AND HIGH LEVEL WASTE MANAGEMENT OPTIONS.
- 05 LA PECHBLENDA DE LA MINA FE (CIUDAD RODRIGO, SALAMANCA), COMO ANÁLOGO NATURAL DEL COMPORTAMIENTO DEL COMBUSTIBLE GASTADO. Proyecto Matrix I.
- 06 TESTING AND VALIDATION OF NUMERICAL MODELS OF GROUNDWATER FLOW, SOLUTE TRANSPORT AND CHEMICAL REACTIONS IN FRACTURED GRANITES: A QUANTITATIVE STUDY OF THE HYDROGEOLOGICAL AND HYDROCHEMICAL IMPACT PRODUCED.
- 07 IV JORNADAS DE INVESTIGACIÓN Y DESARROLLO TECNOLÓGICO EN GESTIÓN DE RESIDUOS RADIACTIVOS. Volumen I.
- 08 IV JORNADAS DE INVESTIGACIÓN Y DESARROLLO TECNOLÓGICO EN GESTIÓN DE RESIDUOS RADIACTIVOS. Volumen II.
- 09 IV JORNADAS DE INVESTIGACIÓN Y DESARROLLO TECNOLÓGICO EN GESTIÓN DE RESIDUOS RADIACTIVOS. Volumen III.
- 10 IV JORNADAS DE INVESTIGACIÓN Y DESARROLLO TECNOLÓGICO EN GESTIÓN DE RESIDUOS RADIACTIVOS. Volumen IV.

2002

- 01 FABRICACIÓN DE BLANCOS PARA LA TRANSMUTACIÓN DE AMERICIO: SÍNTESIS DE MATRICES INERTES POR EL MÉTODO SOL-GEL. ESTUDIO DEL PROCEDIMIENTO DE INFILTRACIÓN DE DISOLUCIONES RADIACTIVAS.
- 02 ESTUDIO GEOQUÍMICO DE LOS PROCESOS DE INTERACCIÓN AGUA-ROCA SOBRE SISTEMAS GEOTERMALES DE AGUAS ALCALINAS GRANITOIDES.
- 03 ALTERACIÓN ALCALINA HIDROTHERMAL DE LA BARRERA DE BENTONITA POR AGUAS INTERSTICIALES DE CEMENTOS.
- 04 THERMO-HYDRO-MECHANICAL CHARACTERISATION OF A BENTONITE FROM CABO DE GATA. A study applied to the use of bentonite as sealing material in high level radioactive waste repositories.
- 05 ESTUDIOS GEOLÓGICO-ESTRUCTURALES Y GEOFÍSICOS EN MINA RATONES (PLUTÓN DE ALBALÁ).
- 06 IMPACTO DE LA MINA RATONES (ALBALÁ, CÁCERES) SOBRE LAS AGUAS SUPERFICIALES Y SUBTERRÁNEAS: MODELIZACIÓN HIDROGEOQUÍMICA.

- 07 CARACTERIZACIÓN PETROLÓGICA, MINERALÓGICA, GEOQUÍMICA Y EVALUACIÓN DEL COMPORTAMIENTO GEOQUÍMICO DE LAS REE EN LA FASE SÓLIDA (GRANITOIDES Y RELLENOS FISURALES) DEL SISTEMA DE INTERACCIÓN AGUA-ROCA DEL ENTORNO DE LA MINA RATONES.
- 08 MODELLING SPENT FUEL AND HLW BEHAVIOUR IN REPOSITORY CONDITIONS. A review of the state of the art.
- 09 UN MODELO NUMÉRICO PARA LA SIMULACIÓN DE TRANSPORTE DE CALOR Y LIBERACIÓN DE MATERIA EN UN ALMACENAMIENTO PROFUNDO DE RESIDUOS RADIACTIVOS.
- 10 PROCESOS GEOQUÍMICOS Y MODIFICACIONES TEXTURALES EN BENTONITA FEBEX COMPACTADA SOMETIDA A UN GRADIENTE TERMOHIDRÁULICO.

2003

- 01 CONTRIBUCIÓN EXPERIMENTAL Y MODELIZACIÓN DE PROCESOS BÁSICOS PARA EL DESARROLLO DEL MODELO DE ALTERACIÓN DE LA MATRIZ DEL COMBUSTIBLE IRRADIADO.
- 02 URANIUM(VI) SORPTION ON GOETHITE AND MAGNETITE: EXPERIMENTAL STUDY AND SURFACE COMPLEXATION MODELLING.
- 03 ANÁLOGOS ARQUEOLÓGICOS E INDUSTRIALES PARA ALMACENAMIENTO DE RESIDUOS RADIACTIVOS: ESTUDIO DE PIEZAS ARQUEOLÓGICAS METÁLICAS (ARCHEO-II).
- 04 EVOLUCIÓN PALEOAMBIENTAL DE LA MITAD SUR DE LA PENÍNSULA IBÉRICA. APLICACIÓN A LA EVALUACIÓN DEL COMPORTAMIENTO DE LOS REPOSITARIOS DE RESIDUOS RADIACTIVOS.
- 05 THE ROLE OF COLLOIDS IN THE RADIONUCLIDE TRANSPORT IN A DEEP GEOLOGICAL REPOSITORY. Participation of CIEMAT in the CRR project.
- 06 V JORNADAS DE INVESTIGACIÓN Y DESARROLLO TECNOLÓGICO EN GESTIÓN DE RESIDUOS RADIACTIVOS. Resúmenes de ponencias.
- 07 V JORNADAS DE INVESTIGACIÓN Y DESARROLLO TECNOLÓGICO EN GESTIÓN DE RESIDUOS RADIACTIVOS. Sinopsis de pósters.
- 08 V JORNADAS DE INVESTIGACIÓN, DESARROLLO TECNOLÓGICO Y DEMOSTRACIÓN EN GESTIÓN DE RESIDUOS RADIACTIVOS. Pósters técnicos.
- 09 DISMANTLING OF THE HEATER 1 AT THE FEBEX "IN SITU" TEST. Descriptions of operations
- 10 GEOQUÍMICA DE FORMACIONES ARCILLOSAS: ESTUDIO DE LA ARCILLA ESPAÑOLA DE REFERENCIA.
- 11 PETROPHYSICS AT THE ROCK MATRIX SCALE: HYDRAULIC PROPERTIES AND PETROGRAPHIC INTERPRETATION.

2004

- 01 PLAN DE INVESTIGACIÓN, DESARROLLO TECNOLÓGICO Y DEMOSTRACIÓN PARA LA GESTIÓN DE RESIDUOS RADIACTIVOS 2004-2008.
- 02 ESTUDIO DE LOS PRODUCTOS DE CORROSIÓN DE LA CÁPSULA Y SU INTERACCIÓN CON LA BARRERA ARCILLOSA DE BENTONITA "CORROBEN".
- 03 EFECTO DE LA MAGNETITA EN LA RETENCIÓN DE LOS RADIONUCLEÍDOS EN EL CAMPO PRÓXIMO: CESIO, ESTRONCIO, MOLIBDENO Y SELENIO.
- 04 I^{ra} JORNADAS DE INVESTIGACIÓN Y DESARROLLO TECNOLÓGICO EN GESTIÓN DE RESIDUOS RADIACTIVOS. Volumen I.
- 05 I^{ra} JORNADAS DE INVESTIGACIÓN Y DESARROLLO TECNOLÓGICO EN GESTIÓN DE RESIDUOS RADIACTIVOS. Volumen II.
- 06 I^{ra} JORNADAS DE INVESTIGACIÓN Y DESARROLLO TECNOLÓGICO EN GESTIÓN DE RESIDUOS RADIACTIVOS. Volumen III.
- 07 I^{ra} JORNADAS DE INVESTIGACIÓN Y DESARROLLO TECNOLÓGICO EN GESTIÓN DE RESIDUOS RADIACTIVOS. Volumen IV.

Febex Project Post-mortem Analysis: Corrosion Study

PUBLICACIÓN TÉCNICA 08/2004

Para más información, dirigirse a:



Dirección de Comunicación
C/ Emilio Vargas, 7
28043 MADRID

<http://www.enresa.es>

Agosto 2004